Global sensitivity analysis of a one-dimensional ocean biogeochemical model

Nabir Mamnun[1], Christoph Völker[1], Sebastian Krumscheid[2], Mihalis Vrekoussis[3,4,5], and Lars Nerger[1]

[1]Alfred-Wegener-Institut (AWI), Helmholtz Zentrum für Polar- und Meeresforschung, Bremerhaven, Germany
[2]Steinbuch Centre for Computing, Karlsruhe Institute of Technology (KIT), Karlsruhe, Germany
[3]Institute of Environmental Physics (IUP), University of Bremen, Bremen, Germany
[4]Center of Marine Environmental Sciences (MARUM), University of Bremen, Bremen, Germany
[5]Climate and Atmosphere Research Center (CARE-C), The Cyprus Institute, Nicosia, Cyprus

Abstract

Ocean biogeochemical (BGC) models are a powerful tool for investigating ocean biogeochemistry and the global carbon cycle. The potential benefits emanating from BGC simulations and predictions are broad, with significant societal impacts from fisheries management to carbon dioxide removal and policy-making. These models contain numerous parameters, each coupled with large uncertainties, leading to significant uncertainty in the model outputs. This study performs a global sensitivity analysis (GSA) of an ocean BGC model to identify the uncertain parameters that impact the variability of model outputs most. The BGC model Regulated Ecosystem Model 2 is used in a one-dimensional configuration at two ocean sites in the North Atlantic (BATS) and the Mediterranean Sea (DYFAMED). Variance-based Sobol' indices are computed to identify the most influential parameters for each site for the quantities of interest (QoIs) commonly considered for the calibration and validation of BGC models. The most sensitive parameters are the maximum chlorophyll to nitrogen ratio, chlorophyll degradation rate, zooplankton grazing and excretion parameters, photosynthesis parameters, and nitrogen and carbon remineralization rate. Overall, the sensitivities of most QoIs were similar across the two sites; however, some differences emerged because of different mixed layer depths. The results suggest that implementing multiple zooplankton function types in BGC models can improve BGC predictions. Further, explicitly implementing heterotrophic bacteria in the model can better simulate the carbon export production and CO_2 fluxes. The study offers a comprehensive list of the most important BGC parameters that need to be quantified for future modeling applications and insights for BGC model developments.

Keywords

Ocean biogeochemical parameters; Regulated Ecosystem Model 2; Sobol' indices; Uncertainty quantification

Code and Data availability

The model and analysis code used in this study are available at https://doi.org/10.5281/zenodo.7685905. Publicly available datasets were used to initiate and force the model. The model outputs are available on request to the corresponding author.

Correspondence:
Contact N. Mamnun at nabir.mamnun@awi.de

Cite this article as:
Mamnun, N., Völker, C., Krumscheid, S., Vrekoussis, M., & Nerger, L.
Global sensitivity analysis of a one-dimensional ocean biogeochemical model
Socio-Environmental Systems Modelling, vol. 5, 2023, doi:10.18174/sesmo.18613

Socio-Environmental Systems Modelling
An Open-Access Scholarly Journal
http://www.sesmo.org

1. Introduction

Ocean biogeochemical (BGC) processes play a central role in shaping our climate by absorbing and sequestering atmospheric carbon dioxide (CO_2). Improving our ability to predict the climate and assess the impacts of climate change on the ecosystems requires a comprehensive understanding of the ocean BGC processes and how they relate to the global climate. Numerical Ocean BGC models are, in addition to measurements, the primary tools for investigating ocean BGC processes and their effects on the carbon cycle and marine ecosystem functioning. BGC models are essential to earth system models used to generate climate projections (Orr et al., 2017) and estimate the global carbon budget (e.g., Hauck et al., 2020). Ocean BGC model outputs can also support management decisions and policy-making in the marine environment and fisheries (e.g., Fennel et al., 2019; Lavoie et al., 2021). For example, they can be used to assess the economic impacts of climate change on fisheries (Tommasi et al., 2017), and provide information on how to mitigate the future effects. BGC models have been used to forecast marine ecosystems operationally (e.g., Gutknecht et al., 2019) and generate reanalysis datasets (e.g., Carroll et al., 2020).

The evaluation of these models involves a wide variety of complex biological and chemical processes described by often simplified schemes in models known as parameterizations. Hence, ocean BGC models include numerous parameters. The values of these parameters are often poorly constrained by theory or observation and are not precisely known. The uncertainty of these parameter values is substantial (Schartau et al., 2017) and, in turn, translates into possibly significant uncertainty in the model outputs. The values of these parameters are usually constrained only from the limited field data or laboratory experiments but usually not in the ocean basin of interest. Therefore, modelers must adjust and tailor model parameters and configuration in each application case (Wagener & Pianosi, 2019) to calibrate the BGC model using observational data, either manually or through optimization algorithms that minimize the misfit between simulations and available data. Focusing on the most influential parameters for the model outputs of interest is crucial to ensure robust and high-quality model prediction. Quantifying the uncertainty caused by these parameters is essential to improve the reliability of the models. Identifying the most relevant input parameters using a computationally cheap one-dimensional (1D) setup permits significant computational savings compared to a three-dimensional (3D) global-scale one by putting numerical effort into the appropriate parameters.

Further developments and improvements of these models are essential to advance our understanding of ocean BGC processes and ensure greater model realism. Sensitivity analysis (SA) is a well-established tool to identify the most influential model parameters and critical relationships within a system, to guide model assessments, and navigate model development (Wagener & Pianosi, 2019; Razavi et al., 2021), especially in a policy context (Saltelli & Funtowicz, 2014). BGC simulations and predictions are used to assess the current state and develop new strategies for mitigating, adapting, and protecting socio-ecological systems. These require adequate uncertainty assessment that provides decision-makers and the public with the necessary information to assess the impact of policy decisions. In turn, uncertainty assessment in model predictions and analysis requires proper uncertainty quantification of model parameters.

SA methods have commonly been divided into two broad categories, namely local sensitivity analysis (LSA), where input factors are varied one at a time (OAT) around the reference values, and global sensitivity analysis (GSA), which assesses the behavior of model outputs by perturbing the entire space of input parameters. In developing and applying the marine BGC models, SA has seldom been performed and reported (e.g., Leles et al., 2018; Chien et al., 2020) and is usually not an integral part of a new modeling application (Prieur et al., 2019). The most common approach in BGC modeling is to conduct a local analysis with a few experiments by varying the parameter values OAT or simultaneously (e.g., Baklouti et al., 2006; Kriest et al., 2012; Kvale & Meissner, 2017).

Some studies assessed the adjoint sensitivity (e.g., Fennel et al., 2001; Tjiputra & Winguth, 2008; Ji et al., 2015) of model output to its inputs by computing gradients. However, it is important to understand that gradient-based SA is a local method because the gradient is a local notion computed in the vicinity of the parameter's current value. Therefore, this gradient, which is a way to quantify the influence of a parameter on model outputs, can be quite

different depending on the chosen value of the parameters. To address this, Sobol' & Kucherenko (2009) introduced derivative based global sensitivity measures (DGSM).

Variance-based sensitivity indicators, in particular so-called Sobol' indices (Sobol', 2001; Saltelli et al., 2004) are widely recognized and popular GSA measures (see Razavi et al., 2021) which provide comprehensive insight into a system's behavior by quantifying each input's contribution to output variance (first-order indices), including their interactions (total-order indices), across the entire parameter space (Saltelli et al., 2008). The computation of Sobol' indices requires a massive number of model evaluations to explore the entire parameter space, which increases exponentially with the number of parameters for grid-based approaches.

As indicated above, ocean BGC models involve numerous parameters, usually several times more than the state variables, ranging from half a hundred to a few hundred. The high number of parameters in the ocean BGC models make GSA computationally very expensive. Therefore, a preliminary screening analysis, such as the OAT screening approach introduced by Morris (1991), is usually carried out to reduce the number of input dimensions before a GSA based on Monte Carlo sampling is performed (e.g., Sankar et al., 2018; Wang et al., 2018). DGSMs, regarded as extensions of the Morris method (Morris, 1991) and related to Sobol' total-order indices (Sobol' & Kucherenko, 2009; Sobol' & Kucherenko, 2010), have been widely employed for screening across various fields. However, the application of DGSM in ocean BGC models remains unexplored. Another way to limit the number of model evaluations to a few thousand is to implement a gradient-informed sampling to compute Sobol' indices (e.g., Leles et al., 2018; Andersen et al., 2021). Nonetheless, Prieur et al. (2019) showed that implementing a direct Monte Carlo sampling-based GSA is feasible for ocean BGC models. Some studies used additional techniques of GSA, such as Gaussian emulators or machine learning approaches (e.g., Scott et al., 2011).

The high demand for computational resources of GSA is why LSA is typically preferred over GSA in ocean BGC models. However, LSA can lead to misleading conclusions and, thus, to a misunderstanding of the influence of every individual process on the simulation results (Prieur et al., 2019). On the other hand, most of the GSA studies for ocean BGC models considered a small set of input parameters due to being computationally expensive. With the increasing availability of computational resources and advances in the GSA algorithms, it is now possible for the scientific community to make GSA the first choice, mainly when dealing with highly parameterized models (Prieur et al., 2019).

This study uses a high-performance computer to make the GSA of an ocean BGC model with a large set of parameters feasible. The GSA focused on computing the sensitivity measures of its input parameters. We consider the BGC model Regulated Ecosystem Model 2 (REcoM2, Hauck et al., 2013) in a one-dimensional configuration at two ocean sites for which observational time series data are available: 1) the Bermuda Atlantic Time-series Study (BATS, Steinberg et al., 2001) in the North Atlantic; and 2) the DYFAMED station (Marty, 2002) in the Mediterranean Sea. The GSA aims to identify the parameters whose uncertainty impacts the variability of BGC model outputs. We compute variance-based Sobol' indices (Sobol', 2001; Saltelli et al., 2004) to assess the most influential parameters for each location for different model outputs that are commonly considered for calibration and validation of BGC models.

2. Biogeochemical Models

Biogeochemistry deals with the exchange and transformations of chemical matter mediated by biological activity within and between reservoirs of the Earth system. In the marine environment, biogeochemistry focuses on the uptake and cycling of carbon and nutrients, e.g., nitrogen, phosphorus, silicon, and iron, between the ocean's organic and inorganic compartments. Therefore, ocean BGC models represent how these chemical species are converted from inorganic matter into organic matter and vice-versa. They are spatially explicit models consisting of components that describe the ocean's physical environment (e.g., temperature and salinity), the marine ecosystem (e.g., phytoplankton, zooplankton), the cycling of inorganic and detrital matter, and air-sea interactions and gas transfer.

Ocean BGC models are generally a set of nonlinear equations of marine physical, biogeochemical, and ecological processes (see Franks, 2002; Fennel et al., 2022) that are translated into computer code, with each equation expressing how each component of the model (e.g., the biomass of phytoplankton) changes with time due to the hydrodynamical effects (e.g., ocean circulation and mixing) and to fluxes between the various components of the marine ecosystem. The common form of these equations is:

$$\frac{\partial C}{\partial t} = dynamics + SMS(C) \tag{1}$$

Here C represents the concentration of a given biological state variable for instant nutrients or the biomass of phytoplankton groups; $dynamics$ includes the advection and transport processes affecting the concentration of C. The term $SMS(C)$, where SMS stands for sources minus sinks, represents the changes of C due to biological processes, air-sea gas exchange, atmospheric deposition, sediment-water exchange, river input, and any transport not arising from ocean circulation, such as the vertical sinking of organic matter.

The SMS components of BGC models describe how ocean biology converts inorganic into organic matters and vice-versa. Phytoplankton takes up inorganic elements, i.e., carbon, nitrogen, silicate, phosphorus, and iron, as nutrients. They gain energy from the sunlight using photosynthesis and convert the inorganic elements into organic ones when they grow. In turn, zooplankton consumes phytoplankton. When phytoplankton and zooplankton die, they sink as part of the detrital matter to the depth where most parts are remineralized back to inorganic form, and the rest are consumed by benthos - organisms that live at or near the bottom of the ocean.

One of the simplest forms of ocean BGC models is the nutrient–phytoplankton–zooplankton–detritus (NPZD) model (see Franks, 2002). It represents how the elements (commonly nitrogen) flow from inorganic nutrients (N) to phytoplankton (P), to zooplankton (Z), how organic matter ends up in a non-living organic pool (detritus, D), and how it is remineralized back to the inorganic pool (Figure 1).

In NPZD models, only nitrogen is typically processed as it is either available as an inorganic nutrient or present in phytoplankton, zooplankton, or detritus in organic form. Carbon and phosphorus are assumed to be in the Redfield ratios (Carbon:Nitrogen:Phosphorus = 106:16:1, Redfield, 1934) with nitrogen. The NPZD model describes the concentration of the four variables (N, P, Z, D) in a homogeneous volume or box by ignoring the physical term $dynamics$. Consequently, the equations are simplified to rate equations for the four state variables. Assuming a closed system, the terms on the right-hand side of the equation reflect transformations between the state variables.

$$\frac{dN}{dt} = \text{remineralization} - \text{uptake} \tag{2}$$

$$\frac{dP}{dt} = \text{uptake} - (\text{assimilated grazing}^1 + \text{sloppy feeding}^2 + \text{phyto. mortality}) \tag{3}$$

$$\frac{dZ}{dt} = \text{assimilated grazing} - (\text{excretion} + \text{zoo. mortality}) \tag{4}$$

$$\frac{dD}{dt} = \text{sloppy feeding} + \text{phyto. mortality} + \text{excretion} + \text{zoo. mortality} - \text{remineralization} \tag{5}$$

The conversions of variables are mass conserving, with gain in one component to another balanced by a corresponding loss. Also, the four equations make a coupled system of equations because the terms on the right-hand side depend on multiple state variables. A simplified scheme describes each BGC transformation, referred to as parameterization.

[1]Marine zooplankton consume a portion of phytoplankton, which refers to *assimilated grazing*.

[2]The unconsumed parts are released as dissolved or particulate organic matter, which refers to *sloppy feeding*.

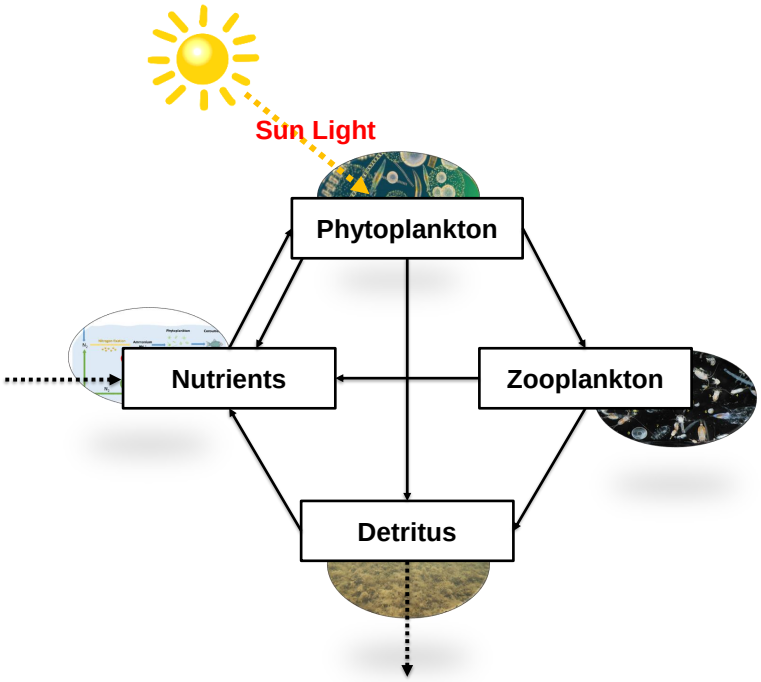

Figure 1: Schematic of a typical NPZD model with its compartments of nutrients, phytoplankton, zooplankton, and detritus. The elements (e.g., N) flow from the inorganic nutrients to phytoplankton, to zooplankton, produce nonliving organic matter detritus, and remineralize back to the inorganic pool. Arrows between compartments indicate the fluxes between them. The dotted arrows imply boundary interactions with the atmosphere and the ocean floor.

The parameters are defined using conceptual understanding from laboratory experiments, field studies, and biological theory (Franks, 2002).

Most current ocean BGC models are extensions of the basic NPZD framework, including more complex BGC model components. Additional state variables include multiple nutrients such as nitrate, ammonium, phosphate, silicate, and dissolved iron; dissolved organic matters, e.g., dissolved organic carbon and nitrogen; numerous phytoplankton and zooplankton functional groups; dissolved gases, for example, oxygen; dissolved inorganic carbon and related properties such as alkalinity.

Ocean BGC models often employ simplified plankton grouping, often referred to as plankton functional types (PFTs, Baretta et al., 1995), for example, diatoms (silicifying phytoplankton), diazotrophs (nitrogen fixers), etc. Organism size is frequently used to differentiate between different PFTs, such as micro-, meso- and macrozooplankton. Multiple PFTs are included to account for the biogeochemically distinct roles played by different functional groups.

Multiple nutrients are needed to address spatial and temporal switches between limiting nutrients and unique requirements by some functional phytoplankton groups, such as diatoms. Many ocean BGC models use the standard Redfield ratios of organisms and fluxes within the marine food web. This simplification allows models to use a single element (e.g., carbon, nitrogen, or phosphorus) as “currency”, which reduces computational costs substantially. However, there are significant deviations around this Redfield stoichiometry (Martiny et al., 2013). A deeper understanding of the drivers of these deviations has enabled the development of a growing number of models with dynamic

stoichiometry (Daines et al., 2014; Ward et al., 2012). This dynamism comes with a computational cost; each element within each PFT needs a variable rather than tracking a single nutrient currency for each. Chlorophyll is usually included within the models to compare the output to satellite ocean color data. Chlorophyll concentrations are often represented in the model by dynamic chlorophyll to carbon ratios (Geider et al., 1998). Due to photoacclimation, the chlorophyll to carbon ratio can vary by one order of magnitude (Fennel & Boss, 2003). Many, but not all, BGC models account for variations in the chlorophyll to carbon ratio using a parameterization of photoacclimation (Geider et al., 1997).

Including the inorganic carbon cycle is crucial for any ocean BGC model used for climate studies (Orr et al., 2017), which requires state variables presenting for dissolved inorganic carbon and alkalinity unless alkalinity can be inferred from other state variables, typically salinity. Including these two properties enables the calculation of other carbonate system properties, such as the partial pressure of carbon dioxide (pCO_2), which is required to parameterize air-sea gas exchange and pH. The latter is of considerable interest, given concerns about ongoing ocean acidification. Another standard state variable in ocean BGC models is oxygen because of its relevance for ecosystem health and functioning.

Ocean circulation and mixing are essential for redistributing the inorganic and organic tracers and plankton (phytoplankton and zooplankton). As such, these models must include a representation of ocean currents, mixing, temperature, salinity, and density. Vertical mixing is particularly important as it controls the supply of nutrients from deep waters to the euphotic zone where phytoplankton grow. The transformations between BGC state variables are connected to their advective and dispersive transport arising from ocean circulation by partial differential equations of the general form given by Equation 1, which can be rewritten for each state variable C:

$$\frac{\partial C}{\partial t} = -u \cdot \nabla_3 C + \nabla_2 \cdot k_H \nabla_2 C + \frac{\partial}{\partial z}\left(k_V \frac{\partial C}{\partial z}\right) + SMS\left(C\right) \tag{6}$$

Here, $u \cdot \nabla_3 C$ represents the advective transport of the constituent C (u is the fluid velocity vector), the terms $\nabla_2 \cdot k_H \nabla_2 C$ and $\frac{\partial}{\partial z}\left(k_v \frac{\partial C}{\partial z}\right)$ represent dispersion in the horizontal and vertical directions, respectively. The parameters k_H and k_V are the horizontal and vertical dispersion coefficients, respectively, while $\nabla_3 = \left(\frac{\partial}{\partial x}, \frac{\partial}{\partial y}, \frac{\partial}{\partial z}\right)$ and $\nabla_2 = \left(\frac{\partial}{\partial x}, \frac{\partial}{\partial y}\right)$ are three-dimensional and two-dimensional operators, respectively. The combination of the first three terms on the right-hand side is referred to simply as $dynamics$ in Equation 1. As physical transport processes operate in all three spatial directions, Equation 6 is three-dimensional in space and includes partial derivatives to time, t, and the three spatial dimensions, x , y, and z. In addition to the equation of this form for each BGC state variable, ocean BGC models include partial differential equations for the physical state variables, including temperature, salinity, and velocity, and parameterizations for horizontal and vertical dispersion coefficients, which can vary in space and time.

Except for a few highly idealized cases — for example, when considering only one spatial dimension or a circular or rectangular two-dimensional domain with homogeneous initial conditions and constant forcing — the solution to these equations cannot be obtained analytically and must be approximated numerically (Glover et al., 2011). The equations are discretized using finite differences in time with time steps Δt on a three-dimensional grid representing the model domain. In the finite-difference methods, the derivatives in the differential equations are replaced by finite difference approximations; for instance, $\frac{\partial C}{\partial t}$ and $\frac{\partial C}{\partial x}$ become $\frac{\Delta C}{\Delta t}$ and $\frac{\Delta C}{\Delta x}$, respectively. Replacing the differential equations leads to a system of prognostic equations, which include only basic arithmetic operations on defined quantities that can be carried out on a computer (Glover et al., 2011).

2.1 Regulated Ecosystem Model 2

In this study, we consider the BGC model Regulated Ecosystem Model 2 (REcoM2, Hauck et al., 2013). REcoM2 describes two phytoplankton classes, diatoms, and nanophytoplankton, with an implicit representation of calcifiers and a generic heterotrophic zooplankton class (Figure 2). It has one class of organic sinking particles whose sinking speed increases with depth and a class of organic matters.

REcoM2 simulates 22 passive tracers (see Figure 2). The intracellular stoichiometry of carbon, nitrogen, calcite and chlorophyll (Carbon:Nitrogen:Chlorophyll) pools for nanophytoplankton and carbon, nitrogen, silicate, and chlorophyll (Carbon:Nitrogen:Silica:Chlorophyll) pools for diatoms are allowed to respond dynamically to environmental conditions following Geider et al. (1998) and Hohn (2009) for the silicate quota. The intracellular iron pool is a function of the intracellular nitrogen concentration (fixed Iron:Nitrogen), as iron is physiologically mainly linked to nitrogen metabolism and the photosynthetic electron transport chain (Geider & La Roche, 1994; Behrenfeld & Milligan, 2013). Dead organic matter is transferred to detritus by aggregation and grazing by one zooplankton class, and the sinking and advection of detritus are represented explicitly. The model has two external iron sources: atmospheric dust deposition and sedimentary input. The iron cycle in the model is driven by biological uptake, remineralization, and scavenging onto biogenic and lithogenic particles. There are 68 BGC parameters in REcoM2 which are summarized in Supplementary Material A.

3. Global sensitivity analysis

Many mathematical models involve input parameters that are not precisely known. GSA aims to identify the parameters whose uncertainty influences the variability of a Quantity of Interest (QoI) most - for instance, by computing Sobol' indices. Let our model output of interest be Y, which is, in abstract terms, a function of the vector of the distributed parameters, $\vec{X} = \{X_1, X_2, X_3, \cdots, X_n\}$ with $n = |\vec{X}|$, i.e.,

$$Y = f\left(\vec{X}\right) = f\left(X_1, X_2, X_3, \cdots, X_n\right) \tag{7}$$

3.1 Uncertainty Propagation

Sources of uncertainties in a mathematical model can be multifold, especially for complex models like ocean BGC. Since the scope of GSA is to identify which model parameters are most influential in the variability of QoIs, we project all uncertainties onto the model input parameters. The main idea is to propagate uncertainties through the model by perturbing the parameters to determine the QoI's sensitivities with respect to these uncertainties. We use the Monte Carlo method, where distribution functions determine the range and probability of parameter values for uncertain parameters.

Deterministic numerical integration encounters problems if the underlying function has many variables. The number of function evaluations required increases exponentially with the number of dimensions, sometimes called the 'curse of dimensionality.' The Monte Carlo method breaks out of this dimensional constraint by solving the definite multidimensional integral for a QoI probabilistically. Such modification will turn the inherently deterministic model into a stochastic one.

In order to describe the domain of uncertainty, we define a probability space for the parameters of $\vec{X}$ by assigning suitable probability density functions $r(\vec{X})$. The respective probability functions $r(\vec{X})$ enable us to formulate the expected value of Y, $\mathbb{E}[Y]$ which can be written mathematically as:

$$\mathbb{E}[Y] \equiv \int_{\Omega_n} f\left(\vec{X}\right) r\left(\vec{X}\right) d\vec{X} \tag{8}$$

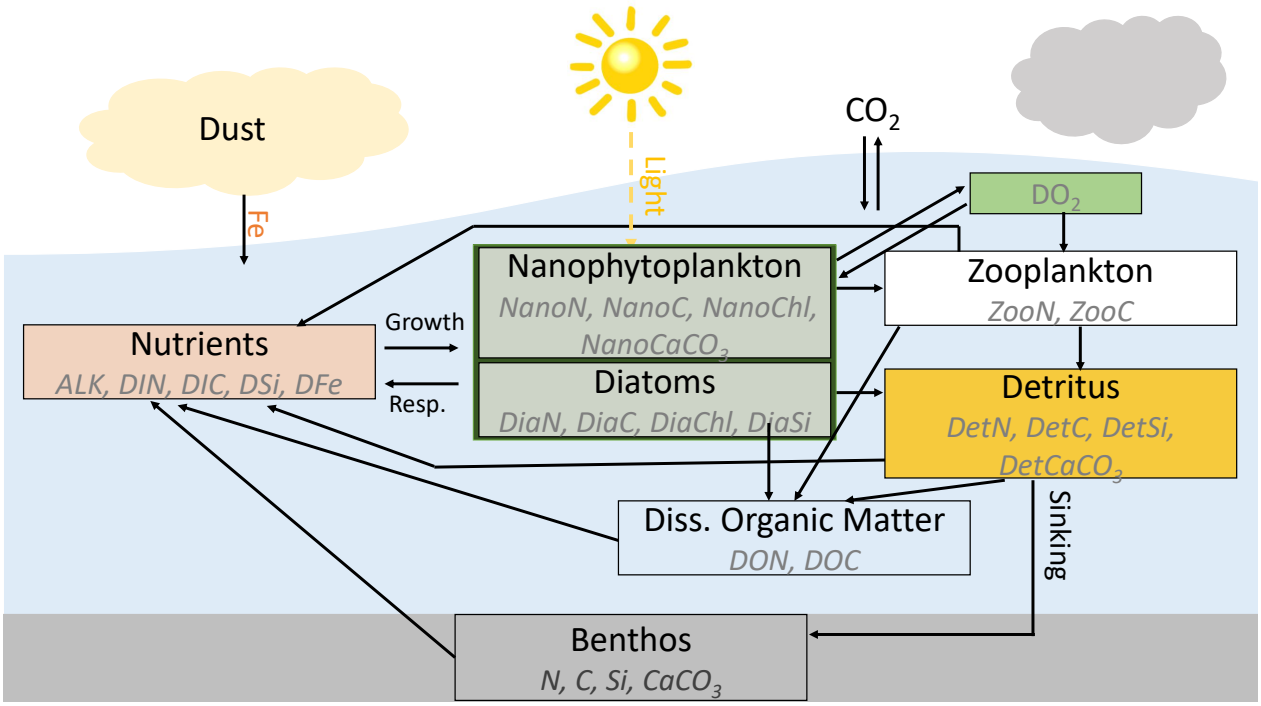

Figure 2: Schematic diagram of the BGC model REcoM2. The abbreviations are for the 22 passive tracers – dissolved inorganic carbon (DIC) and alkalinity (ALK) for the carbonate system; the macro-nutrients dissolved inorganic nitrogen (DIN) and silicic acid (DSi); the trace metal dissolved iron (DFe), nanophytoplankton biomass content of carbon (NanoC), nitrogen (NanoN), calcium carbonate ($NanoCaCO_3$) and chlorophyll (NanoChl); diatoms biomass content of carbon (DiaC), nitrogen (DiaN), silica (DiaSi) and chlorophyll (DiaChl); zooplankton biomass content of carbon (ZooC), nitrogen (ZooN); detritus content of carbon (DetC), nitrogen (DetN), silicate (DetSi) and calcium carbonate ($DetCaCO_3$); extra-cellular dissolved organic carbon (DOC) and nitrogen (DON); and dissolved oxygen (DO_2). Arrows depict source and sink terms.

where $\Omega_n \subseteq \mathbb{R}^n$ is the parameter domain in the n–dimensional hypercube. However, without loss of generality we assume that $\Omega_n \subseteq [0,1]^n$ instead of $\mathbb{R}^n$ since all parameters can be, in theory, mapped to the n-dimensional unit hypercube thanks to the inverse transformation method.

3.2 Derivative-based Global Sensitivity Measure (DGSM)

DGSM is a model independent GSA approach that examines the relative influence of different model parameters on a given QoI by calculating the expected value of the square of the derivative of the function f with respect to that parameter.

Let $f : \mathbb{R}^n \to \mathbb{R}$ and denoted by $\frac{\partial f\left(\vec{X}\right)}{\partial X_i}$ its partial derivative with respect to the input parameter X_i evaluated at $\vec{X} = (X_1, X_2, \cdots, X_n)^T \in \mathbb{R}^n$. The DGSM, as defined by Sobol' & Kucherenko (2009), with respect to the i-th input can be written as

$$DGSM_i \equiv \mathbb{E}\left(\frac{\partial f}{\partial X_i}\left(\vec{X}\right)\right)^2 = \int \left(\frac{\partial f}{\partial X_i}\left(\vec{X}\right)\right)^2 r\left(\vec{X}\right) d\vec{X} \tag{9}$$

Here, $\mathbb{E}$ denotes the expected value of the squared partial derivative with respect to the input X_i and $r(\vec{X})$ is the probability density functions of $\vec{X}$.

The principle underlying this approach is that the parameters that cause larger variations in the model output will have larger derivatives, and hence, will have larger DGSM values. Therefore, the DGSM value provides an indication of the relative influence of the input parameters on the output.

For simple and differentiable models the derivative may be directly calculated using calculus. However, for more complex models, particularly those involving non-differentiable functions, or many input parameters like ocean BGC, one needs to resort to numerical methods to approximate the derivative. The most common approach is the finite difference method, which involves calculating the change in the model output for a small perturbation in the parameter of interest:

$$\frac{df}{dX_i} \approx \frac{f\left(X_1, \cdots, X_i, X_i + \Delta X_i, \cdots, X_n\right) - f\left(X_1, \cdots, X_i, X_i - \Delta X_i, \cdots, X_n\right)}{2\Delta X_i} \tag{10}$$

where, ΔX_i is a small increment to the parameter X_i while the other input parameters remain unchanged.

3.3 Variance-based sensitivity measures

Since we treat the input parameters $\vec{X} = \{X_1, X_2, \cdots, X_n\}$ as random variables, the model response Y is turned into stochastic due to the uncertainty in $\vec{X}$, although the integral is deterministic. The overall uncertainty in the sense of variability (or spread) in Y caused by $\vec{X}$ is the variance of Y, $Var[Y]$. We are interested in variance-based sensitivity measures that quantify how much of $Var[Y]$ can be attributed to each X_i, for $i \in \{1, 2, \cdots, n\}$.

The Sobol' indices (Sobol, 1993) were first introduced to measure the sensitivity of the output to each of the inputs X_i. Under the assumption of independent inputs, $Var[Y]$ is decomposed as a sum of variance components attributable to each X_i. Homma & Saltelli (1996) define the first-order Sobol' index, S_i of X_i as

$$S_i \equiv Var\left[\mathbb{E}\left[Y|X_i\right]\right] = Var\left[Y\right] - \mathbb{E}\left[Var\left[Y|X_i\right]\right] \tag{11}$$

By definition, S_i leaves out the variability of Y caused by interactions of X_i with other inputs. The right-hand side of Equation 11 can be interpreted as the expected reduction in $Var[Y]$ when we fix the value of X_i to a constant. To complement the first-order Sobol' index Homma & Saltelli (1996) define the total-order Sobol' index T_i of X_i as

$$T_i \equiv Var\left[Y\right] - Var\left[\mathbb{E}\left[Y|X_{\sim i}\right]\right] = \mathbb{E}\left[Var\left[Y|X_{\sim i}\right]\right] \tag{12}$$

where $X_{\sim i}$ denotes the vector of all input parameters $\vec{X}$ except X_i. Here, T_i is the expected variance that remains in Y when the values of every parameter except X_i could be fixed to a constant.

These two Sobol' indices are widely used and are a robust measure of parameter sensitivity. The first- and total-order sensitivity indices can be related to the objectives of GSA (Saltelli et al., 2004, 2008). The first-order Sobol' index, also known as the main effect (Homma & Saltelli, 1996), tells us how much variance of model output Y, $Var[Y]$, can be reduced when we fix the respective parameter. The sum of the first-order Sobol' indices can not exceed 1 (Glen & Isaacs, 2012). Therefore, in the case of a large set of input parameters, the first-order Sobol' indices of many input parameters are close to 0, and the corresponding parameters have low main effects. The main effects or total-order Sobol' indices are relevant to parameter prioritization in identifying the most influential parameter since fixing a parameter to a constant with the highest index value would, on average, lead to the most significant reduction in

the output variation. However, a low first-order Sobol' sensitivity index value does not imply that the model output is independent of the input parameter X_i as it does not capture the interaction with other parameters (Plischke et al., 2013; Saltelli et al., 2008).

The total-order Sobol' indices, also known as the total effects (Homma & Saltelli, 1996), provide us with the sensitivity due to interactions among a given parameter X_i and all other parameters. The total-order index is relevant in identifying the least influential parameters since fixing any parameter with a minimal total effect would not significantly reduce output variation. Therefore, using the total-order Sobol' index to identify which parameter can be excluded for surrogate modeling would be more exact, though computationally expensive.

GSA sometimes includes a screening step to reduce the computational burden, as Saltelli et al. (2008) recommended. The screening step aims to identify all non-influential parameters conditional on the chosen QoI and concentrate the detailed GSA on influential parameters. We also applied this approach in this study. After screening, we deal with uncertainty propagation, where some values of $\vec{X}$ are considered to be uncertain while others are not. We thus split the input into a vector $\vec{\chi}$ of undisturbed parameters and a vector $\vec{x}$ of parameters screened as uncertain, i.e., $\vec{X} = (\vec{\chi}, \vec{x})$, which enable us to reformulate $\mathbb{E}[Y]$ with regard to $\vec{X}$:

$$\mathbb{E}\left[f\left(\vec{\chi}, \vec{x}\right)\right] \equiv \int_{\Omega_d} f\left(\vec{\chi}, \vec{x}\right) r\left(\vec{x}\right) d\vec{x} \tag{13}$$

in contrast to Equation 8 we integrate over the function of vector $\vec{x} = (x_1, x_2, \cdots, x_d)$. The integral bounds are, therefore, only d–dimensional here.

3.4 Computing of Sobol' indices

For simple models, SA can be done analytically by directly computing the first- and total-order effects according to Equations 11 and 12. However, this is generally prohibitive for complex models like ocean BGC. In those cases, one evaluates the model with perturbed input parameter values and then uses the resulting output values to estimate sensitivity indices of interest using suitable sample averages. Many different estimation procedures of the Sobol' indices have been proposed and studied. However, the traditional method has two big drawbacks. First, it relies on a particular experimental design that may be unavailable in practice. Second, its computational cost may be prohibitive when estimating several indices. Naturally, the cost of an estimator depends on the cost of each evaluation of the computational model and the number of evaluations. For the traditional estimator, the number of model calls for all the first-order Sobol' indices grows linearly with the number of input parameters. For most of the traditional estimators, the number of required model evaluations is $(n + 2) \times N$, where n is the number of input parameters and N is the sample size (i.e., the number of perturbed input parameter replica).

In recent years a few estimators have been developed to estimate the first-order global sensitivity indices with only N number of model evaluations, for example, the random balance designs method (Tarantola et al., 2006) or double loop reordering approaches proposed by Kucherenko & Song (2017). Gamboa et al. (2022) presented an estimator based on rank statistics using an empirical correlation coefficient introduced by Chatterjee (2020), which can estimate the first-order Sobol' indices with a unique N-sample, thus, N model evaluations. We applied the estimator developed by Gamboa et al. (2022) to compute first-order Sobol' indices in this study. For total-order Sobol' indices, we utilized the nearest neighbor search proposed in Broto et al. (2020), which needs only N model evaluations.

3.5 Implementation in this study

In this study, we used a 1D coupled hydrodynamic-biogeochemical model. In the coupled model, the Massachusetts Institute of Technology General Circulation Model (MITgcm, Marshall et al., 1997) simulates ocean dynamics and tracer transport, while REcoM2 (see Section 2.1) handles ocean BGC processes and transformation. MITgcm is a finite volume, general circulation model with a non-hydrostatic capability that allows the model to be used for describing small-scale to global-scale processes. REcoM2 is coupled with MITgcm as a combined model system.

We used the identical model set-up of Mamnun et al. (2022). A 1D configuration of the coupled MITgcm-REcoM2 was set up at two ocean sites, BATS in the North Atlantic Ocean and DYFAMED in the Mediterranean Sea, for which observational time series data are available. Both stations are in an oligotrophic environment, i.e., exhibiting low primary production.

The 1D water column model consists of 30 vertical layers. The vertical grid intervals increase as the depth increases, starting at 10 meters near the surface and reaching 100 meters near the lowermost layer, encompassing a total model depth of 1188 meters. Since we focus on ecosystem processes within the euphotic zone and their connection to vertical nutrient transport from the mesopelagic, we have restricted our model configuration to slightly over the upper 1000 meters, ensuring ample distance from the seabed at both sites. The model time step was 1 hour (3600 seconds).

The model temperature, salinity, DO_2, DIN, and DSi fields were initialized with in situ bottle data. We obtained in situ data for BATS from its website (`https://bats.bios.edu/`) and for DYFAMED from Coppola et al. (2021). We initialized the ALK and DIC fields of the model from the mapped climatology of the GLobal Ocean Data Analysis Project (GLODAPv2, Lauvset et al., 2016) at both sites, and DFe with data from the U.S. GEOTRACES North Atlantic Transect (GA-03, Boyle et al., 2015) at BATS and from the data reported in Guieu & Blain (2013) at DYFAMED. We initialized all other passive tracers with small uniform values. We force the model with inter-annually varying atmospheric forcing data from the Coordinated Ocean Research Experiments version 2 (COREv2, Large & Yeager, 2008) for BATS and ERA5 (Hersbach et al., 2020) single levels data for DYFAMED. We used the monthly dust deposition field from the present-day simulation of Albani et al. (2014) to compute DFe input flux from the atmosphere, assuming 3.5% iron content in dust particles and 2% solubility.

As mentioned above, REcoM2 includes 68 uncertain input parameters. Our model does not touch the ocean bottom; therefore, we excluded the five parameters related to the benthic layer. In REcoM2, the linear slope of Arrhenius function is fixed to 4500, therefore, we also excluded this parameter from our analysis. We considered the remaining 62 parameters for the GSA.

The first step to implement a GSA was to propagate uncertainties into the model by perturbing the input parameters applying the Monte Carlo method. We assume that each parameter has some predefined reference value. The uncertainties address relatively small deviations. It is plausible to employ a probability density function where the statistical properties of mean, median, or mode lie close to the reference value and where values are more improbable the more they diverge from the reference value. Such intuition naturally excludes uniform or exponential distributions, for example. A commonly used distribution for this purpose is the normal distribution. With a normal distribution $N(1, \sigma^2)$ for some standard deviation, we would center its bell curve to 1 such that uncertainties are realized by a factor multiplication of the reference value with a normally distributed variable. However, a normal distribution may not be suitable for BGC parameters. Campbell (1995) demonstrated that log-normal statistics reasonably describe many BGC variables (e.g., chlorophyll concentrations) in the ocean. Therefore, a common distribution used for BGC parameters is the log-normal distribution. Furthermore, BGC parameters are always positive quantities. Utilizing the log-normal parameter guarantees the positiveness of parameter values. Notably, some BGC parameters are ratio of quantities and constrained between 0 and 1, thus assumed to follow a beta distribution.

The Monte Carlo approach samples points uniformly at random on a unit hypercube Ω_n. In this study, we employ the

pseudo-random number generator, `random`, embedded in the core Python library (van Rossum & the Python development team, 2022) for generating random numbers. We transformed the random values onto a probability density function in the interval $[0; 1)$. For the transformation, we specified a probability distribution for each input parameter with the following assumption.

1. The uncertainties of the various parameters are independent.
2. The ratio parameters constraining value between 0 and 1 follow a beta distribution.
3. The parameter "reference temperature" follows a normal distribution.
4. Other parameters follow a log-normal distribution.
5. The standard deviation of the distribution is 50% of their reference value.

We used a sample size of one hundred thousand (10^5). Therefore, the Monte Carlo method gave 10^5 sets of parameter values. The sample size 10^5 was chosen, guided by a convergence test.

Application of a quasi-Monte Carlo (qMC) method based on low discrepancy sequences (e.g., Sobol' sequences) often surpasses the performance of standard Monte Carlo methods by several orders of magnitude, which manifests a noteworthy decrease in the number of necessary model evaluations (Kucherenko et al., 2011; Kucherenko & Song, 2017; Ökten & Liu, 2021). However, a preceding study (Thelen, 2021) has demonstrated that despite the better convergence rate of qMC compared to the standard Monte Carlo, the qMC based Sobol' sequences sometimes give negative or unreasonably high values of Sobol' indices for REcoM2 model parameters. Although demanding in computation resources, a standard Monte Carlo method-based sampling for GSA has become affordable, thanks to the advancements of high-performing computers.

The next step was to evaluate the model for each parameter set. We performed model simulations for ten years (1990–1999) at both stations and saved time-average output values every five days. To minimize the effects of model initialization, we excluded the first five years of simulations as a spin-up period (1990–1994). The output values were processed across the analysis period of the later five years (1995–1999).

Running the ocean BGC model several thousand times is computationally very costly despite using a 1D column model. The high demand for computational resources is why LSA is typically preferred in practice over GSA for ocean BGC models. For computationally expensive ocean BGC models with many parameters, applying a standard Monte Carlo method-based sampling for GSA is often not feasible due to the necessity for a substantial sample size. In this study, we make GSA tractable with a large set of parameters using a high-performance computer. A single model simulation took around 5 minutes using one processor core. Using 960 cores (10 compute nodes) of the computer we were able to perform 100,000 simulations in about 9 hours.

We computed Sobol' indices using the `R` package `sensitivity` (Iooss et al., 2022). Though, the estimator used in this study allows us to compute the total-order Sobol' indices with $N = 10^5$ model evaluations, with all 62 model parameters, the estimator needs a very large matrix for computing the total-order Sobol' indices. This makes it impractical to compute the total-order Sobol' indices for all 62 parameters, even in a high-performance computer.

To reduce the computational burden, we carried out a screening step using first-order Sobol' indices and DGSM. The screening step aims to identify all influential and non-influential parameters on the chosen QoIs and concentrate the detailed GSA on influential parameters Saltelli et al. (2008).

We computed DGSMs utilizing the Python library Sensitivity Analysis Library (SALib, Herman & Usher, 2017; Iwanaga et al., 2022). We drew samples using the qMC (Sobol') sequence combined with the finite difference approach with small increment, as implemented in the SALib for each input parameter. The abovementioned probability distribution with a 50% standard deviation determined the bounds of parameter values. The sample size was 1000.

The screening step identified 28 uncertain parameters (see section 4.1) for which we computed both first- and total-order Sobol' indices. Note that the screening step is essential for a traditional method as it reduces the number of input parameters, thus reducing the requirements of high number $N \times (n + 2)$ of model runs, where n is number of input parameters.

3.6 Quantities of interest

One defines the QoIs according to the primary scientific objectives of the sensitivity study. We considered QoIs that are commonly used for the calibration and validation of BGC models as our QoIs. GSA applies to scalar output quantities. Therefore, to apply the GSA method, we reduced the time variations of QoIs to scalar indicators by time-averaging. The QoIs considered in the study are listed in Table 1.

Table 1: Quantities of interest chosen for the present study.

QoI	Description
SURF_TOTCHL	Mean surface total chlorophyll
SURF_NANOCHL	Mean surface nanophytoplankton chlorophyll
SURF_DIACHL	Mean surface diatom chlorophyll
MBP_TOTCHL	Annual peak surface total chlorophyll
MBP_NANOCHL	Annual peak surface nanophytoplankton chlorophyll
MBP_DIACHL	Annual peak surface diatom chlorophyll
TOTNPP	Mean net primary production (NPP)
NANONPP	Mean nanophytoplankton NPP
DIANPP	Mean of Annual diatom NPP
EXPORTC	Annual mean export production of carbon
pCO_2	Mean partial pressure of CO_2
CO_2FLUX	Mean surface flux of CO_2

4. Results

4.1 Screening step

In the screening step, we estimated the first-order Sobol' indices and their 95% confidence interval for all 62 parameters regarding each QoI at both locations. The first-order Sobol' indices for mean surface chlorophyll at both stations are presented in Figure 3(a). As we used a large sample size ($N = 10^5$), the 95% confidence intervals are close to zero and not visible in a plot therefore not shown in Figure 3(a). A threshold value of 0.02 clearly separates the high and low first-order indices (Figure 3(a)).

Only ten parameters have a first-order index greater than the threshold value of 0.02 against mean surface chlorophyll at least one station (Figure 3(a)). We obtained similar results for the other QoIs (see Supplementary Material B). 26 model parameters have a first Sobol' index greater than 0.02 for at least one of the QoIs and for at least one station.

However, employing first-order Sobol' indices to screen out non-influential parameters has certain limitations. Specifically, it can result in erroneous conclusions (Sobol' et al., 2007) as the first-order index of a parameter does not account for its interaction with other parameters. A parameter with a negligible estimated first-order Sobol' index may still have a high total-order index due to significant interactions with other parameters, and thereby the parameter remains influential to the variability of model outputs. To address this concern, we supplemented the screening using first-order

indices with DGSM, given its global nature and relation with Sobol' total order indices (Sobol' & Kucherenko, 2009). We computed DGSMs and their 95% confidence interval of all 62 parameters for each of the QoIs. Figure 3(b) shows DGSMs and their 95% confidence interval for mean surface chlorophyll (SURF_TOTCHL).

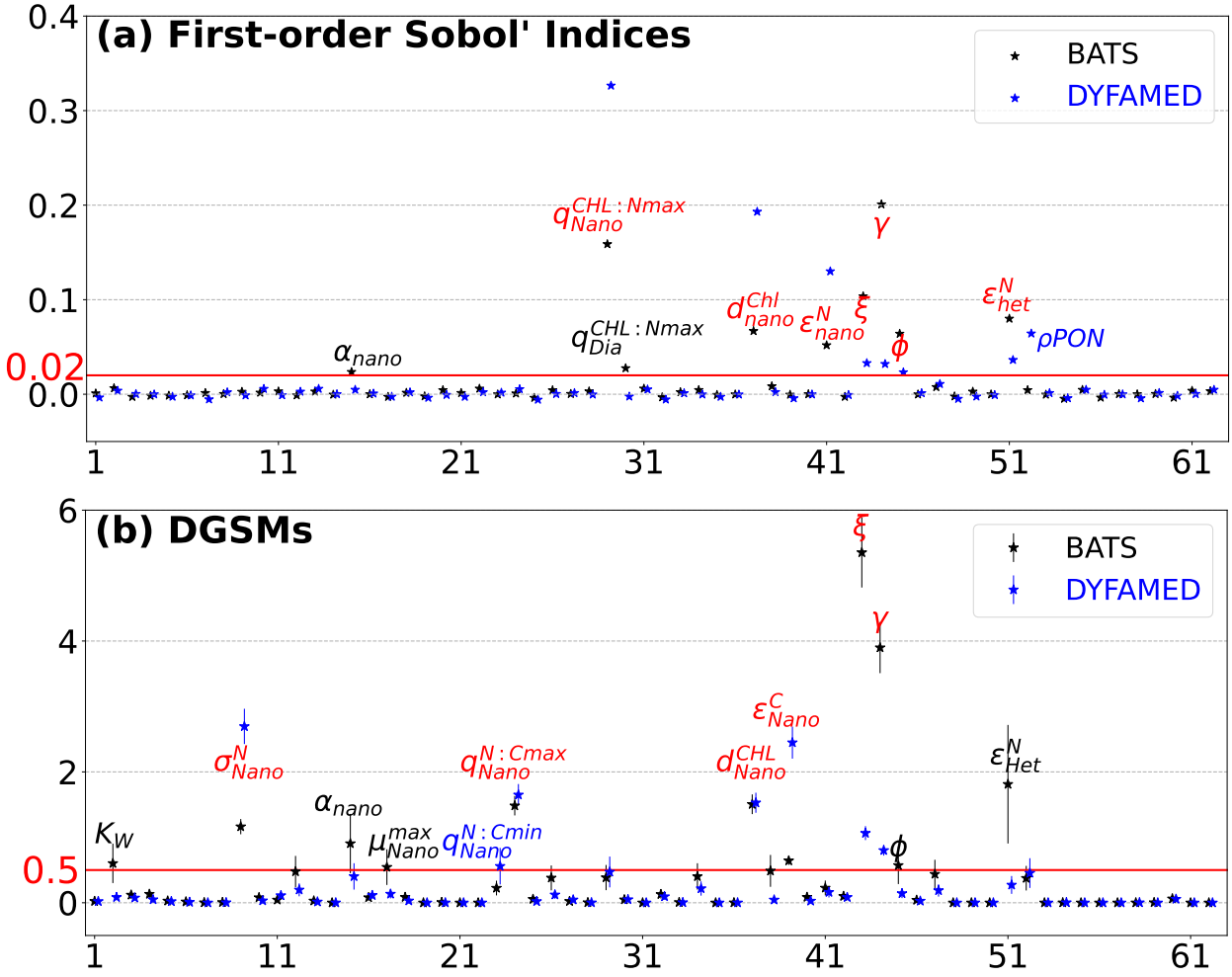

Figure 3: (a) First-order Sobol' indices and **(b)** DGSMs and their 95% confidence interval of 62 parameters for mean surface chlorophyll (SURF_TOTCHL). In both plots, parameters for which the sensitivity measures are greater than the threshold value at both stations are written in red, at only BATS in black, and at only DYFAMED in blue. The x-axis labels are the serial number of parameters in Supplementary Material A.

Similar to Sobol' first-order indices we can identify a threshold value that clearly separates the high and low DGSM. In case of DGSM the threshold value is 0.5, much higher than the one for first-order indices because of their interaction effects. Overall, the important parameters are the same except for nitrogen uptake ratio (σ^{N}_{Dia}) and the minimum cell quota of nitrogen for nanophytoplankton, which have high DGSMs but low Sobol' first-order indices at both stations. On the other hand, nanophytoplankton maximum chlorophyll to nitrogen ratio ($q^{CHL:Nmax}_{Nano}$) has high first-order indices but low DGSMs.

We applied an approach analogous to the one previously employed for screening parameters through the utilization of

Sobol' first-order indices to DGSMs. Similar to Sobol' first order indices only 12 parameters exhibit high DGSM values for SURF_TOTCHL and can be distinctly separated by a threshold value of 0.5 (see Figure 3(b)). Through the utilization of DGSM, we shortlisted 26 parameters. It is noteworthy that each approach shortlisted two uncommon parameters to each other. Figure 4 summarizes the number of QoI for which the estimate of the first-order Sobol' index and DGSMs exceeded the threshold value. We merged both approaches and shortlisted 28 parameters based on the fact that they are influential for at least one chosen QoI at least at one station. The shortlisted parameters are presented in Table 2.

Table 2: Shortlisted parameters for which the first-order Sobol' indices are greater than 0.02 for at least one QoI at any one station.

Parameter	**Description**
K_W	Light attenuation coefficient
K^N_{Nano}	Nanophytoplankton half-saturation constant for nitrogen uptake
K^N_{Dia}	Diatom half-saturation constant for nitrogen uptake
σ^N_{Nano}	Nanophytoplankton nitrogen to carbon uptake ratio
σ^N_{Dia}	Diatom nitrogen to carbon uptake ratio
V^{Nmax}_{Nano}	Nanophytoplankton maximum nitrogen uptake
α_{Nano}	Nanophytoplankton initial slope of P-I curve
α_{Dia}	Diatom initial slope of P-I curve
μ^{max}_{Nano}	Nanophytoplankton maximum photosynthesis rate
μ^{max}_{Dia}	Diatom maximum photosynthesis rate
$q^{N:Cmin}_{Nano}$	Nanophytoplankton minimum cell quota of nitrogen (N:C)
$q^{N:Cmax}_{Nano}$	Nanophytoplankton Maximum cell quota of nitrogen (N:C)
$q^{N:Cmax}_{Dia}$	Diatom Maximum cell quota of nitrogen (N:C)
$q^{CHL:Nmax}_{Nano}$	Nanophytoplankton maximum of chlorophyll to nitrogen ratio
$q^{CHL:Nmax}_{Dia}$	Diatom maximum of chlorophyll to nitrogen ratio
ζ^N_{Nano}	Nanophytoplankton cost of nitrogen biosynthesis
d^{CHL}_{Nano}	Nanophytoplankton chlorophyll degradation rate
d^{CHL}_{Dia}	Diatom chlorophyll degradation rate
ϵ^C_{Nano}	Nanophytoplankton excretion rate of carbon
ϵ^C_{Dia}	Diatom excretion rate of carbon
ϵ^N_{Nano}	Nanophytoplankton excretion rate of nitrogen
ϵ^N_{Dia}	Diatom excretion rate of nitrogen
ξ	Maximum grazing rate by zooplankton
γ	Grazing efficiency of zooplankton
ϕ	Half-saturation constant for grazing
ϵ^N_{Het}	Zooplankton nitrogen excretion rate
ρ_{PON}	Particulate organic nitrogen degradation rate of detritus
ρ_{POC}	Particulate organic carbon degradation rate of detritus

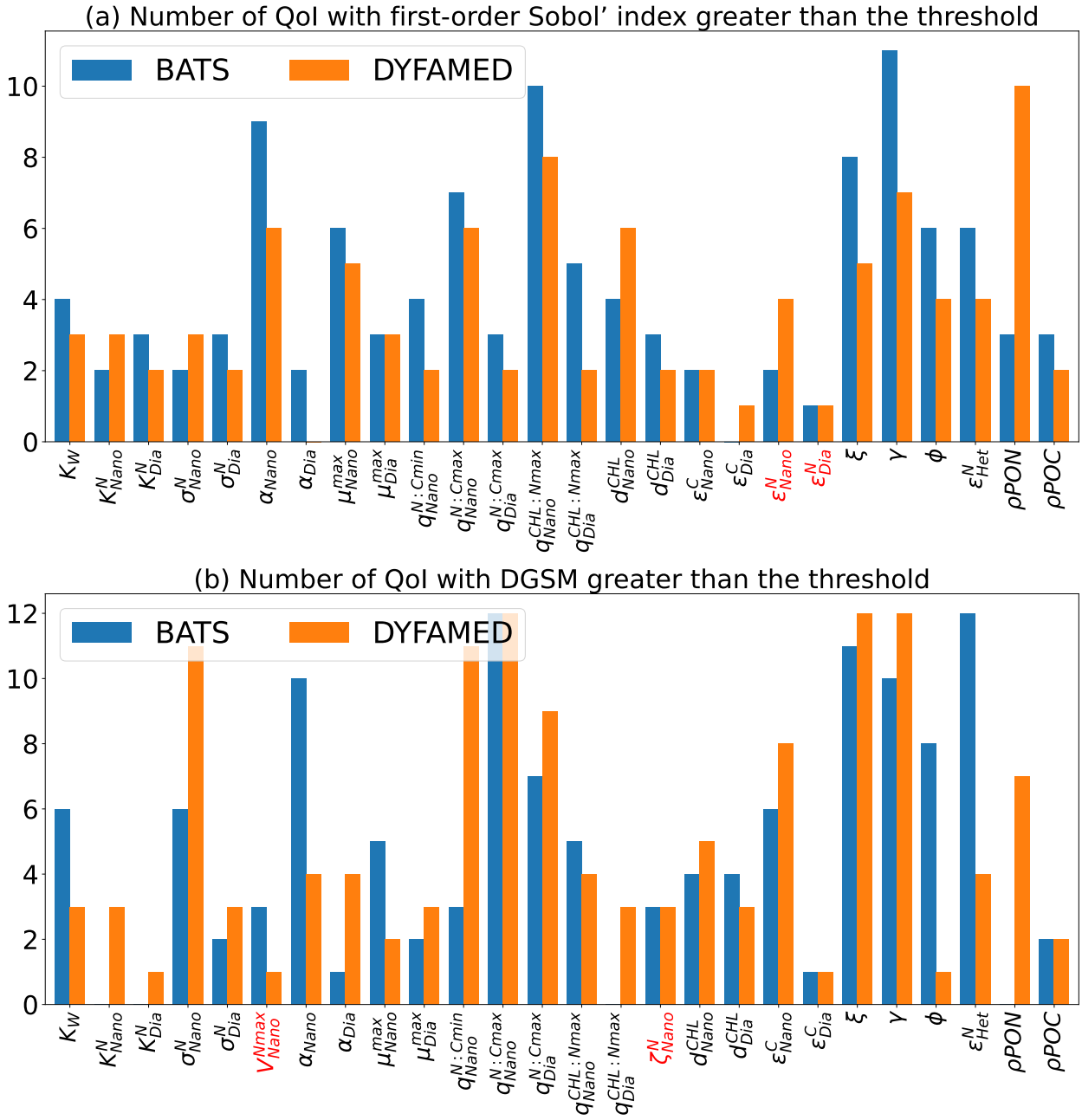

Figure 4: Number (count) of QoIs (y-axis) for which the estimate of **(a)** the first-order index and **(b)** the DGSM exceed a threshold value. Here, for each of the screening approaches, the parameters whose sensitivity measures are larger than the threshold for at least one QoI at any one station are plotted and rest of the parameters whose sensitivity measures stayed within the threshold value for all QoIs at both locations are not shown. The symbol of uncommon parameters in each group is written in red.

4.2 Parameter sensitivity

We computed first- and total-order Sobol' indices of those 26 influential shortlisted parameters for each of the QoIs at both locations. The first-order Sobol' indices of the shortlisted parameters corroborated with the first-order Sobol' indices of the screening step. The relative ranking of the most influential parameters was consistent for all the QoIs at both locations.

Figure 5 shows the total-order Sobol' indices of the short-listed parameters for mean surface chlorophyll at both stations. The total-order indices are far larger than the first-order indices. This shows that the parameters contribute to the total variance primarily through their interactions with other parameters. However, it is not possible to define a threshold value for the total-order Sobol' indices. Nonetheless, total-order Sobol' indices provide us with the rank of the most critical parameters and bring important information since input parameters with a very low value for both first-order and total-order Sobol' index can be fixed to a reference value in a calibration procedure. The seven most influential parameters for mean surface chlorophyll, annual peak surface chlorophyll, mean NPP, mean carbon export production and mean pCO_2 with their ranking according to the first- and total-order Sobol' indices are presented in Table 3 for both stations. Though the ranking order differs in the two locations, the top seven influential parameters are more or less similar across both stations.

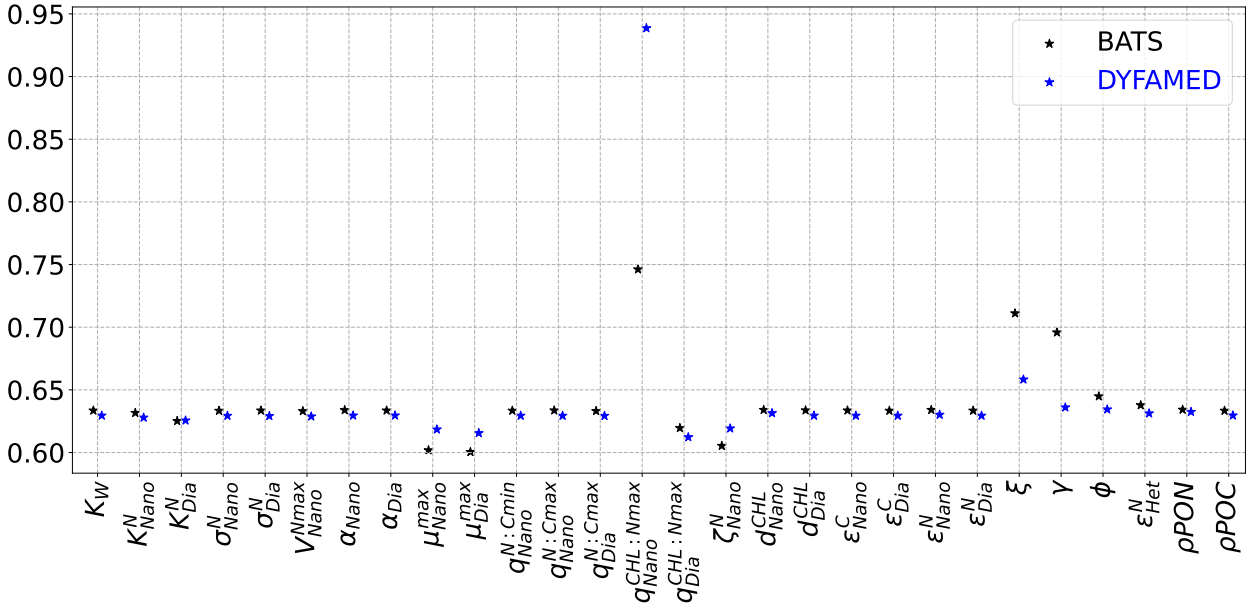

Figure 5: Total-order Sobol' indices of the 26 shortlisted parameters regarding mean surface chlorophyll (SURF_TOTCHL). For a description of the parameters, see Table 2.

Figure 6 shows the first- and total-order Sobol' indices regarding all of the QoIs for each of two stations. As total-order indices are large and not on a similar scale across the two stations, we normalized them for better visibility and comparison; and plotted the normalized values. Overall, the most sensitive parameters are the maximum chlorophyll to nitrogen ratio, chlorophyll degradation rate, zooplankton grazing and excretion parameters, photosynthesis parameters, and nitrogen and carbon remineralization rate.

For the mean surface chlorophyll (SURF_TOTCHL) simulation, the maximum chlorophyll to nitrogen ratio of nanophytoplankton ($q^{CHL:Nmax}_{Nano}$) and two grazing parameters, the maximum grazing rate (ξ) and grazing efficiency (γ) are the

most influential parameters at both stations (Table 3 and Figure 6). At DYFAMED, ξ and γ show less sensitivity for first-order Sobol' indices but are highly influenced by their interactions with other parameters. Other sensitive parameters at BATS are the zooplankton nitrogen excretion rate (ϵ^N_{Het}), the nanophytoplankton chlorophyll degradation rate (d^{CHL}_{Nano}), the half-saturation constant for grazing (ϕ), the nanophytoplankton excretion rate of nitrogen (ϵ^N_{Nano}), the maximum chlorophyll to nitrogen ratio of diatoms ($q^{CHL:Nmax}_{Dia}$), the initial slope of photosynthesis-irradiance curve of nanoplankton (α_{Nano}), diatom chlorophyll degradation rate (d^{CHL}_{Dia}), and the maximum photosynthesis rate of nanophytoplankton (μ^{max}_{Nano}). These parameters are also sensitive at DYFAMED except for two diatom-related parameters, d^{CHL}_{Nano} and d^{CHL}_{Dia}. In addition, the particulate organic nitrogen degradation rate of detritus (ρPON) is also sensitive at DYFAMED (Figure 6).

The sensitive parameters for nanophytoplankton surface chlorophyll (SURF_NANOCHL) are similar to SURF_TOTCHL except for diatom-related parameters. From the model outputs, we found that the diatoms had less than a 10% contribution to the annual mean surface chlorophyll concentration; therefore, it is apparent that the diatom parameters are not sensitive to SURF_NANOCHL. Similar to SURF_NANOCHL, the maximum chlorophyll to nitrogen ratio of diatom is the most influential parameter for the diatom surface chlorophyll (SURF_DIACHL). However, the other sensitive parameters for this QoI vary from SURF_TOTCHL and SURF_NANOCHL at both stations. The grazing parameters show less sensitivity to SURF_DIACHL compared to SURF_NANOCHL. For SURF_DIACHL, some of the nanophytoplankton parameters e.g., α_{Nano}, μ^{max}_{Nano}, $q^{CHL:Nmax}_{Nano}$ and $q^{N:Cmax}_{Nano}$ (nanoplankton maximum cell quota of nitrogen) are also influential at both locations (Figure 6).

$q^{CHL:Nmax}_{Nano}$ was the most influential parameter in determining the annual peak surface chlorophyll (MBP_TOTCHL) at both stations with its main- and total-effects. The other sensitive parameters for MBP_TOTCHL at BATS are $q^{CHL:Nmax}_{Dia}$, the grazing parameters γ, ξ and ϕ, zooplankton excretion parameter ϵ^N_{Het}, and CHL loss parameter d^{CHL}_{Nano}. At DYFAMED, $q^{CHL:Nmax}_{Dia}$ is not sensitive regarding MBP_TOTCHL. The remineralization parameter ρPON shows high sensitivity at BATS. In addition to the above-mentioned parameters α_{Nano}, μ^{max}_{Nano} and $q^{N:Cmax}_{Nano}$ were sensitive for MBP_TOTCHL at both stations. The sensitive parameters for the annual peak nanophytoplankton surface chlorophyll (MBP_NANOCHL) are analogous to MBP_TOTCHL, except for the diatom parameters and slight shifts in ranking. For annual peak surface diatom chlorophyll (MBP_DIACHL), two nanophytoplankton parameters, μ^{max}_{Nano} and α_{Nano} were also sensitive, which highlights the interaction between the two phytoplankton groups (Figure 6). The nanophytoplankton maximum nitrogen uptake (V^{Nmax}_{Nano}) shows sensitivity to MBP_NANOCHL and MBP_TOTCHL when interacting with other parameters at both locations.

For simulating NPP (totnpp in Table 1), the grazing parameters γ, ξ, and ϕ, photosynthetic parameter α_{Nano} and μ^{max}_{Nano}, the zooplankton respiration parameters ϵ^N_{Het}, the nanophytoplankton excretion rate of carbon (ϵ^C_{Nano}), the light attenuation coefficient K_W, and the cell quota $q^{CHL:Nmax}_{Nano}$ and $q^{C:Nmax}_{Nano}$ were sensitive at both locations (Table 3 and Figure 6). In addition d^{CHL}_{Nano} and ρPON were sensitive at DYFAMED. At BATS, γ and ξ had their highest values for both first- and total-order Sobol' indices, whereas at DYFAMED, they have the highest values for total-order Sobol' indices but relatively lower value for first-order indices. Overall, zooplankton parameters are more sensitive at BATS compared to DYFAMED. The influential parameters for total NPP (TOTNPP) and nanophytoplankton NPP (NANONPP) are the same, except for the ranking difference. Comparably, a higher number of parameters showed sensitivity for diatom NPP than other quantities of interest at both stations with the initial slope of photosynthesis–irradiance curve of diatom (α_{Nano}), the diatom maximum photosynthesis rate (μ^{max}_{Dia}) and $q^{CHL:Nmax}_{Dia}$ the most sensitive parameters for diatom NPP (DIANPP). (V^{Nmax}_{Nano}) has a small main effect but a high total effect on NANONPP and TOTNPP at BATS. Similar effects of nanophytoplankton cost of nitrogen biosynthesis (ζ^N_{Nano}) were found at DYFAMED.

The remineralization parameters ρPON and ρPOC are the most influential parameters for the simulation of export production of carbon (EXPORTC) at BATS followed by the photosynthesis parameter α_{Nano}, the cell quota $q^{C:Nmin}_{Nano}$, $q^{C:Nmax}_{Nano}$ and $q^{CHL:Nmax}_{Nano}$, photosynthesis parameter μ^{max}_{Nano} and grazing parameter γ. At DYFAMED, ρPON, γ, $q^{C:Nmin}_{Nano}$ and ξ are the most influential parameters for export production simulation.

The most influential parameters for the simulation of the partial pressure of carbon dioxide (pCO_2) and surface flux of carbon dioxide (CO_2FLUX) are the remineralization rate of nitrogen ρPON and carbon ρPOC, and the light attenuation coefficient (K_W) at BATS. At DYFAMED the most influential parameters are ρPON, ρPOC, $q_{Nano}^{C:Nmax}$ and the grazing parameter γ.

5. Discussion

5.1 Parameter sensitivity across locations

We undertook a GSA with variance-based sensitivity methods to analyze the sensitivity of model outputs in a 1D configuration of the ocean BGC model MITgcm-REcoM2 for two ocean locations. Overall, the sensitivity responses of most of the QoIs were similar between the two locations. However, some differences emerged, which can be attributed to the availability of nutrients and, specifically, continuous upwelling and strong convective mixing differing mixed layer depth.

Surface chlorophyll is often the first choice of model output for calibration and validation of ocean BGC models, as it can be compared to satellite ocean color products that are widely available and have good spatial coverage. In REcoM2, chlorophyll synthesis is coupled with nitrogen uptake, with its rate being proportional to nitrogen uptake by phytoplankton (Hauck et al., 2013). The chlorophyll synthesis is represented by the cell quota, the maximum chlorophyll to nitrogen ratio for the respective phytoplankton group ($q_{Nano}^{CHL:Nmax}$ for nanophytoplankton and $q_{Dia}^{CHL:Nmax}$ for diatoms). Therefore, the maximum chlorophyll to nitrogen ratios significantly contribute to the variability of surface CHL. At both locations, $q_{Nano}^{CHL:Nmax}$ has the highest value in both first- and total-order indices. In contrast, $q_{Dia}^{CHL:Nmax}$ has little influence on the total surface chlorophyll simulations because of low diatom contributions to the annual total phytoplankton population in oligotrophic environments. The contribution of diatoms to total surface chlorophyll concentration is generally less than 10% at both stations, which agrees with data from in situ observations from Steinberg et al. (2001) for BATS and Marty et al. (2008) for DYFAMED.

The annual peak surface chlorophyll concentration at BATS is sensitive to $q_{Dia}^{CHL:Nmax}$. Diatom contribution to the total phytoplankton biomass can exceed 30% during the bloom period at this station (Nelson & Brzezinski, 1997). Albeit their low abundance and biomass, diatoms grow actively during the spring bloom period at BATS and have a higher contribution to NPP. REcoM2 chlorophyll production is computed as a function of irradiance and nitrogen uptake. The uptake of nitrogen by the phytoplankton is converted to chlorophyll using the parameters maximum chlorophyll to nitrogen ratio ($q_{Nano}^{CHL:Nmax}$ and $q_{Dia}^{CHL:Nmax}$) . The highest possible chlorophyll synthesis is down-regulated by this ratio, which depends on photosynthesis and light absorption. It increases under low irradiance and decreases as photosynthesis becomes light-saturated. Therefore, during the bloom period, when photosynthesis is significant, changes in this ratio produce a large variability in the chlorophyll synthesis. As diatom photosynthesis is high during bloom peak at BATS, changes in $q_{Dia}^{CHL:Nmax}$ lead to considerable variability in the chlorophyll synthesis. On the other hand, unlike BATS, diatoms are less abundant during the spring bloom at DYFAMED. REcoM2 underestimates diatom production at the station, hence, $q_{Dia}^{CHL:Nmax}$ is not important for the phytoplankton bloom at DYFAMED in our analysis.

As the chlorophyll concentration products derived from satellite ocean color are widely available, chlorophyll is often included in the model as a proxy for living phytoplankton biomass so that the chlorophyll simulation can be used for model validation. Photoinduced and microbial processes lessen chlorophyll before the phytoplankton are grazed or die. The overall chlorophyll loss, in turn, contributes to phytoplanktonic carbon loss. Therefore, loss of chlorophyll from functional cells is necessary in REcoM2, and is parameterized by a fixed chlorophyll degradation rate (d_{Nano}^{CHL} for nanophytoplankton and d_{Dia}^{CHL} for diatom). These parameters are highly influential for the simulation of surface chlorophyll concentration (Figure 6), which are difficult to constrain by observations (Mamnun et al., 2022). They become even more important during low-growth conditions in winter. The latter is supported by the higher sensitivities

Table 3: Ranking of the seven most influential model parameters on mean surface chlorophyll (SURF_TOTCHL), annual peak surface chlorophyll (MBP_TOTCHL), mean NPP (TOTNPP), mean carbon export production (EXPORTC) and mean pCO_2 from the total-order Sobol' indices.

QoI	Rank	BATS		DYFAMED	
		first-order	total-order	first-order	total-order
SURF_TOTCHL	1	γ	$q_{Nano}^{CHL:Nmax}$	$q_{Nano}^{CHL:Nmax}$	$q_{Nano}^{CHL:Nmax}$
	2	$q_{Nano}^{CHL:Nmax}$	γ	d_{Nano}^{CHL}	ξ
	3	ξ	ξ	ϵ_{Nano}^{N}	γ
	4	ϵ_{Het}^{N}	ϕ	ρPON	ϕ
	5	d_{Nano}^{CHL}	ϵ_{Nano}^{N}	ϵ_{Het}^{N}	ρPON
	6	ϕ	ρPON	ξ	d_{Nano}^{CHL}
	7	ϵ_{Nano}^{N}	α_{Nano}	γ	ϵ_{Nano}^{N}
MBP_TOTCHL	1	$q_{Nano}^{CHL:Nmax}$	$q_{Nano}^{CHL:Nmax}$	$q_{Nano}^{CHL:Nmax}$	$q_{Nano}^{CHL:Nmax}$
	2	γ	$q_{Dia}^{CHL:Nmax}$	ρPON	ρPON
	3	$q_{Dia}^{CHL:Nmax}$	ξ	d_{Nano}^{CHL}	ξ
	4	ξ	γ	α_{Nano}	d_{Nano}^{CHL}
	5	ϕ	ϕ	ϕ	ϕ
	6	ϵ_{Het}^{N}	V_{Nano}^{Nmax}	ϵ_{Nano}^{N}	α_{Nano}
	7	d_{Nano}^{CHL}	ϵ_{Nano}^{N}	γ	V_{Nano}^{Nmax}
TOTNPP	1	γ	γ	α_{Nano}	ξ
	2	ξ	ξ	ϵ_{Nano}^{C}	γ
	3	α_{Nano}	ϕ	ρPON	μ_{Nano}^{max}
	4	μ_{Nano}^{max}	ϵ_{Het}^{N}	ξ	ϕ
	5	ϵ_{Nano}^{C}	α_{Nano}	ϵ_{Het}^{N}	$q_{Nano}^{CHL:Nmax}$
	6	ϕ	μ_{Nano}^{max}	$q_{Nano}^{CHL:Nmax}$	α_{Nano}
	7	ϵ_{Het}^{N}	V_{Nano}^{Nmax}	γ	ζ_{Nano}^{N}
EXPORTC	1	ρPON	ρPON	ρPON	ρPON
	2	ρPOC	$q_{Nano}^{CHL:Nmax}$	γ	γ
	3	$q_{Nano}^{N:Cmin}$	ρPOC	$q_{Nano}^{N:Cmax}$	$q_{Nano}^{N:Cmax}$
	4	$q_{Nano}^{N:Cmax}$	μ_{Nano}^{max}	ξ	ρPOC
	5	$q_{Nano}^{CHL:Nmax}$	α_{Nano}	ρPOC	σ_{Nano}^{N}
	6	μ_{Nano}^{max}	$q_{Nano}^{N:Cmax}$	ϵ_{Het}^{N}	ϵ_{Nano}^{N}
	7	γ	γ	ϕ	ϵ_{Dia}^{N}
pCO_2	1	ρPOC	ρPOC	ρPON	ρPON
	2	γ	ρPON	ρPOC	ρPOC
	3	ρPON	γ	$q_{Nano}^{N:Cmax}$	$q_{Nano}^{N:Cmax}$
	4	$q_{Nano}^{N:Cmax}$	ϕ	$q_{Nano}^{N:Cmin}$	σ_{Nano}^{N}
	5	$q_{Nano}^{N:Cmin}$	α_{Nano}	γ	ϵ_{Nano}^{N}
	6	ξ	α_{Dia}	ϕ	ϵ_{Dia}^{N}
	7	α_{Nano}	ϵ_{Het}^{N}	ϵ_{Het}^{N}	ϵ_{Het}^{N}

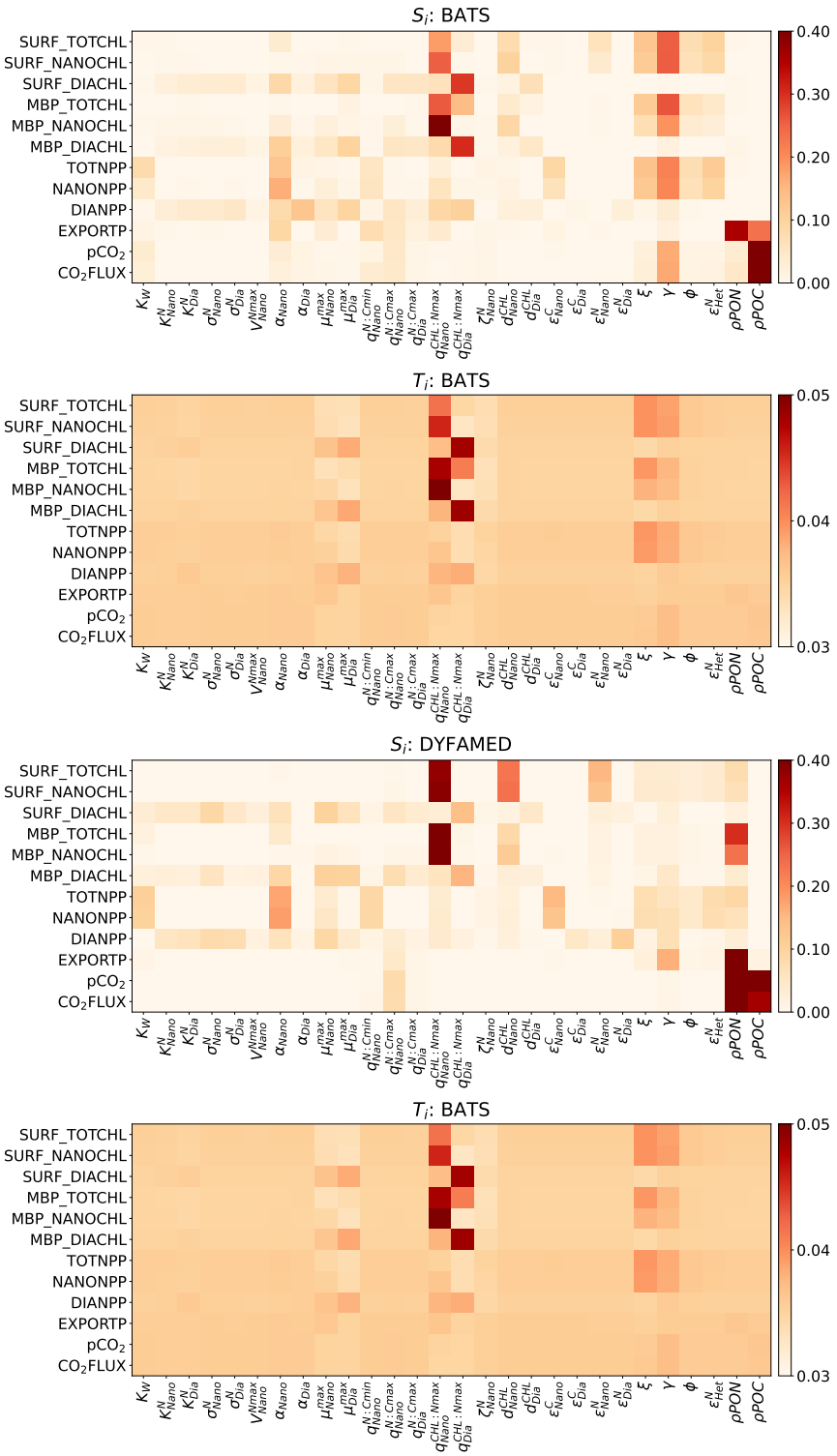

Figure 6: First- and total-order Sobol' sensitivity indices of the short-listed parameters regarding all included QoIs at both stations. For better visibility, the total-order Sobol' indices were normalized. For a description of QoI and parameters, see Table 1 and Table 2, respectively.

computed for the annual mean surface chlorophyll compared to the mean peak surface chlorophyll. The chlorophyll loss term, in reality, describes processes in senescent or photo-stressed cells, thus playing a pivotal role in phytoplankton carbon to chlorophyll ratios (Álvarez et al., 2018). Our results suggest that replacing the simple chlorophyll degradation model with a more process-based description of the degradation of photosystem functionality can lead to improved modeled carbon to chlorophyll ratios and should be pursued further, as also indicated in Álvarez et al. (2018).

Our study emphasizes the importance of the parameters describing the zooplankton grazing process, such as ξ, γ and ϕ for BGC simulations (Figure 6). Zooplankton grazing is vital in the ocean food web and biogeochemical cycles (see Steinberg & Landry, 2017). The grazing parameters in ocean BGC models strongly impact the phytoplankton dynamics and nutrient cycling processes (Le Quéré et al., 2016; Anderson et al., 2013; Karakuş et al., 2022). They regulate the phytoplankton biomass in the photic zone, thus controlling the biological production and the carbon and nutrients uptake by photosynthesis. Previous sensitivity studies of ocean BGC models (e.g., Tjiputra et al., 2007; Prieur et al., 2019; Bracis et al., 2020; Chien et al., 2020) indicated that zooplankton grazing parameters are very sensitive BGC parameters for simulated variables related to phytoplankton dynamics. Chenillat et al. (2021) showed that small changes in grazing rate greatly affect the plankton ecosystem model. Makler-Pick et al. (2011) performed a GSA study by including three zooplankton groups in a BGC model and did not find zooplankton grazing parameters as the most influential sloppy feeding and grazing rate of zooplankton was overall sensitive, though. REcoM2 parameterized only one zooplankton group to represent the entire zooplankton community and its impact on the marine ecosystem. As most zooplankton communities vary across space and time, a single zooplankton group might provide a too limited description of the grazing process of an entire ecosystem. Increasing the number of zooplankton groups would likely weaken the sensitivity of grazing parameters, which suggests that implementing multiple zooplankton function types in BGC models would likely improve chlorophyll and NPP simulation, provided that efforts are invested in estimating parameters characterizing the grazing in marine ecosystems. It has been shown (Karakuş et al., 2022) that representing multiple zooplankton groups in an ocean BGC model strongly impacts the seasonal dynamics of phytoplankton, food web structure, and elemental cycles.

The grazing parameters show stronger sensitivity at BATS compared to DYFAMED. In addition to being grazed by zooplankton, in REcoM2, phytoplankton mortality is represented by non-physiological terms such as aggregation. The aggregation is assumed to be proportional to phytoplankton abundance, becoming more important during the spring bloom period. In REcoM2, mortality dominates the loss process compared to grazing in nutrient-abundant areas (Laufkötter et al., 2016). The grazing parameters strongly influence BGC simulations at BATS because zooplankton consumes most of the primary production at this location, consistent with in situ measurements reported by Evelyn & Michael (1998). At BATS, reduced ξ increases phytoplankton biomass in the euphotic zone, thus increasing nutrient uptake by photosynthesis. As grazing parameters are less sensitive at DYFAMED compared to BATS, the aggregation parameters should have some sensitivity (Laufkötter et al., 2016) at DYFAMED. However, our sensitivity analysis shows that aggregation parameters do not have much influence on the phytoplankton dynamics at DYFAMED. This suggests that the aggregation parameterization does not properly represent the phytoplankton mortality process at the station. It is likely that explicitly representing phytoplankton mortality as physiological mortality can improve the simulation in oligotrophic regions. The effect of grazing parameters at DYFAMED increases when they interact with other parameters. Increasing influence because of interaction indicates strong co-dependencies of zooplankton grazing on phytoplankton dynamics and nutrient cycling.

The GSA shows that the zooplankton nitrogen excretion rate, ϵ^N_{Het} is sensitive to BGC simulations. The rate ϵ^N_{Het} mainly controls the DON released by zooplankton. In addition, DON concentration is reduced when ϵ^N_{Het} is small, reducing the amount of organic matter that is immediately recycled into nutrients in the euphotic zone. Hence, the parameter influences the balance between new and regenerated nitrogen, which affects the BGC cycle. An increase in ϵ^N_{Het} reduces zooplankton biogenic concentration. It thus increases the flux of regenerated nitrogen, which leads to an increase in primary production, chlorophyll concentration and nitrogen assimilation. However, the zooplankton

excretion rate of carbon ϵ^C_{Het}, did not show sensitivity in our analysis. In the oligotrophic regions, the zooplankton excretion of carbon regulates primary production by supplying regenerated nutrients, especially when the zooplankton concentration is high (Popova et al., 2006). Druon & Le Fèvre (1999) found that increasing the zooplankton excretion rate of carbon in a BGC model could enhance primary productivity. Since ϵ^C_{Het} impacts the zooplankton biomass, it would also help control the grazing pressure, hence sloppy feeding, over a more extended period. Over longer time scales, changes in HetC would influence regenerated nutrients, which would change photosynthesis and carbon uptake, but that is not evident in our analysis. One reason is that carbon content loss from zooplankton is dominated by carbon-rich fecal pellets of macrozooplankton (Karakuş et al., 2022), which our model does not represent explicitly. The representation of macrozooplankton fecal pellets and their contribution to sinking particles are significant in ocean BGC models (Laufkötter et al., 2016). Our results highlight the critical role of macrozooplankton in the carbon and nutrient cycles. Thus, representing macrozooplankton in the BGC model would improve future projections of carbon cycling.

The photosynthesis parameters maximum growth rate (μ^{max}) and initial slope of photosynthesis-irradiance curve (α) show sensitivity at both stations. Annual upwelling and intense convective mixing maintain a seasonal supply of essential nutrients to the surface for phytoplankton growth at both locations (Sweeney et al. (2003) for BATS; Marty et al. (2008) for DYFAMED). Because of atmospheric dust input, iron availability does not limit phytoplankton growth either at BATS (Nelson & Brzezinski, 1997) or at DYFAMED (Mayot et al., 2020). Therefore, the increasing growth rate increases photosynthesis. However, the GSA suggests that photosynthesis parameters have a low sensitivity on export production at the two sites investigated here, though these processes are essential for DIC in general (Olsen et al., 2008). In our study, the parameters related to phytoplankton growth had relatively low importance for BGC simulations. The low sensitivity of phytoplankton growth parameters can be because the model was implemented in two oligotrophic areas with a fully stratified water column and relatively low primary production. Therefore, the mass of organic matter exported from the surface to the depth is low. In our simulation, the weak connection between the euphotic (productive) zone and the lower layers makes the export production less dependent on phytoplankton growth.

Our study indicates that the surface CO_2 fluxes and pCO_2 are mostly sensitive to the remineralization parameters ρ_{PON} and ρ_{POC}, the grazing parameter γ, and cell quota $q^{N:Cmax}_{Nano}$ and $q^{N:Cmin}_{Nano}$. Remineralization parameters control the dissolved organic matter. An increase in remineralization rate decreases dissolved organic matter concentration at the surface and enhances regenerated nutrients, increasing photosynthesis and carbon uptake. In REcoM2, the remineralization is not regulated by biological processes. It is likely that implementing heterotrophic bacteria explicitly in the model has the potential for an improved simulation of export production and CO_2 fluxes. Reducing γ would substantially increase the uptake of atmospheric CO_2. The results agree with previous sensitivity studies, which indicated that the sea-to-air CO_2 flux and surface pCO_2 are sensitive to grazing parameters.

5.2 First-order vs. total-order Sobol' indices

Figure 7 shows a scatter plot of first-order and total-order indices. The relation between first-order and total indices is not linear. More precisely, the parameters with a high first-order Sobol' index generally have a larger total-order Sobol' index value than those with a low first-order Sobol' index. Nevertheless, this generalization may vary significantly for some parameters. For example, the maximum growth rate corresponds to the largest first-order Sobol' index, which has a total-order index smaller than several other parameters with much smaller first-order indices at BATS. On the other hand, some parameters with a small first-order Sobol' index have a high total-order index.

Note that the sum of first-order Sobol' indices is less than 1 and the sum of total-order Sobol' indices equals far more than 1. This indicates that the BGC models are not additive models of the form of Equation 7. This is due to correlations between different BGC parameters (Mamnun et al., 2022). Co-dependencies between parameters make any simple interpretation of Sobol' indices non-trivial. As mentioned above, computing total-order Sobol' indices may not always

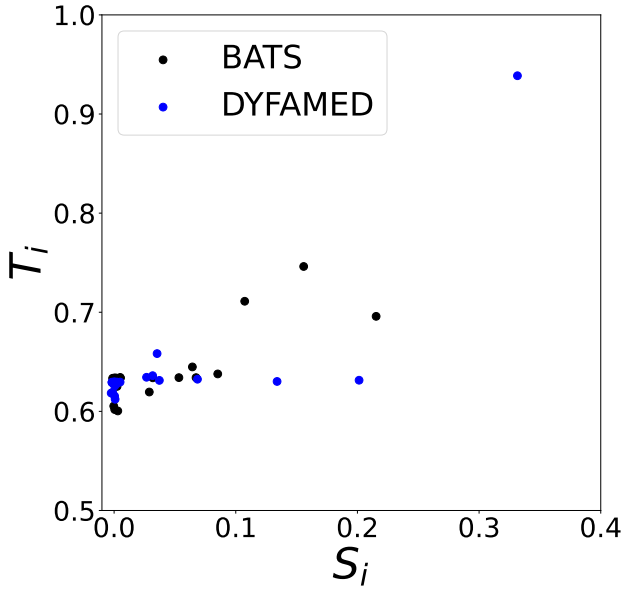

Figure 7: Scatterplot of first-order (x-axis) and total-order (y-axis) Sobol' indices of the short-listed parameters for NPP

be affordable, depending on the computational resources available. However, they bring essential information since input parameters with a minimal value for their total Sobol' index can be fixed to a nominal value in a calibration procedure.

The hypothesis of uncorrelated input parameters is common in GSA regardless of the method used (see Razavi et al., 2021). This assumption, however, faces challenges in real-world problems, where it becomes a rare exception to find models without correlated input parameters, particularly in models representing highly complex systems or systems with numerous parameters like those used in earth system modeling. The correlation effect is distinct from the 'total effect,' which denotes the non-additive influence of individual parameters on the QoI (Razavi & Gupta, 2015). The presence of dependent input parameters might indeed induce errors and bias in the GSA outcomes. Yet, they are used to identify the most uncertain parameters and provide vital insights that enhance our understanding of the modeled system which our results also demonstrated. Researchers in various fields frequently utilize Sobol' indices in their models, even when dealing with dependent inputs (e.g., Kalra et al., 2017; Islam & Karadogan, 2019; Prieur et al., 2019). They recognize, however, that overlooking the correlation effects can introduce biases into the results of GSA. This understanding underscores the need for careful consideration and potential adjustment when interpreting the outcomes of such analyses. Recently, some methods have emerged to accommodate correlated inputs, including but not limited to copula-based techniques (e.g., Kucherenko et al., 2012; Sheikholeslami et al., 2021) and applications of game-theory concepts (e.g., Owen et al., 2014; Owen & Prieur, 2017; Iooss & Prieur, 2019). However, these novel methods' applications are still on the horizon for ocean BGC models.

5.3 Implications of our study

Modelers usually rely on previous SA studies for targeted parameters to be tuned during calibration for a new modeling application (see Wagener & Pianosi, 2019). However, most previous SA studies are conducted on a single location, mainly because of computational constraints. The conventional LSA can result in misleading conclusions and, thus, a misinterpretation of the influence of process parameters on the critical model outputs (Prieur et al., 2019). Ocean BGC models contain many parameters, so conducting a GSA for the output of these models is computationally expensive.

Therefore, ocean BGC modelers prefer the LSA to GSA. With the availability of high-performing computing technologies and recent advances in computation algorithms, BGC researchers can apply the GSA methods presented in this study with little effort before any new modeling application. The methods set here can be applied to analyze the sensitivity of other ocean BGC model outputs or QoIs (e.g., dissolved oxygen in surface layers) as well as other locations of the world ocean.

As indicated above, the main aim of GSA is to identify the parameters that have the most impact on a QoI. Thus, GSA helps prioritize the parameters for estimation with data assimilation (see Dowd et al., 2014, for a review of data assimilation into ocean BGC models) which we apply in an ongoing study. In model tuning, it prioritizes the most influential parameters for the model outputs to focus on optimization efforts, that minimize the misfit between simulations and available data, on these few parameters. Before starting with parameter estimation, a preceding GSA could provide helpful information, e.g., selecting only parameters to which the observed variables are sensitive. Likewise, an identifiability analysis could complement the SA by furnishing information on parameter range and possible ambiguities of parameter estimates (Schartau et al., 2017).

GSA could also serve as an additional tool for model evaluation during the calibration of an ocean BGC model. It can provide a system-level assessment (e.g., Leles et al., 2018), assuming that the influential parameters identified by the GSA reflect the most critical processes of interest. Any dissimilarity between observed data and the outcomes of GSA in terms of the most significant process parameters would require an examination into the parameterization and the cause of the discrepancy (see Gupta & Razavi, 2018) and thereby help parameter identification in the ocean BGC model. If the discrepancies come from parameter values, this deserves a new round of calibration. On the other hand, if the discrepancies do not match the current knowledge of the modeled systems, this demands investigation of the model structure and parameterization to better reflect the knowledge of essential processes in the marine ecosystem. For example, at both locations, the aggregation parameters are not influential for any of the QoIs. REcoM2 describes the loss process of phytoplankton by grazing and aggregation, where aggregation dominates grazing (Laufkötter et al., 2016). A recent study by Mamnun et al. (2022) found that aggregation parameters influence the surface chlorophyll concentration at DYFAMED - an increase in the specific aggregation rate of both phytoplankton and detritus decreases surface chlorophyll concentration significantly. Therefore, the absence of influence of aggregation parameters does not correspond with current knowledge of the systems modeled and needs investigations into these parameterizations and maybe changes in the model structure.

6. Conclusion

We performed a GSA of an ocean BGC model concerning the sensitivity of its input parameters. The GSA aimed to understand which model parameters contribute the most to the model uncertainty. We consider the BGC model REcoM2 in a one-dimensional configuration at two ocean sites. We estimated variance-based Sobol' indices for each parameter at both stations. For mean chlorophyll simulations, we found that the maximum chlorophyll to nitrogen ratio, chlorophyll degradation rate, and parameters related to zooplankton grazing and excretion were sensitive at both stations. For predictions of net primary production, the most influential parameters are those related to photosynthesis, zooplankton grazing, and the excretion of organic matter by phytoplankton and zooplankton. Export production of carbon, pCO_2 and surface CO_2 flux are sensitive to mainly the remineralization of nutrients and grazing by zooplankton. The parameters related to diatoms were not significant because the contribution of the phytoplankton group to the overall phytoplankton community was low at both locations.

Our results suggest that implementing multiple zooplankton functional types in BGC models will likely improve chlorophyll and NPP prediction, provided that efforts are invested in estimating parameters characterizing the grazing in marine ecosystems. The GSA indicates that explicitly representing phytoplankton mortality as physiological mortality, currently not used in REcoM2, can improve simulation in oligotrophic regions. Our results also indicate that the ex-

plicit representation of heterotrophic bacteria in the model can potentially improve the simulation of carbon export production and CO_2 fluxes.

Despite the limitation of the one-dimensional model configuration, our application offers a comprehensive list of the most important biogeochemical parameters that need to be quantified for future applications of a global configuration. The insight gained from the GSA will be broadly applicable in future BGC modeling case studies, parameter estimation and optimization, and for further development of BGC models. Stakeholders, policies, and society need reliable information for decision-making, not only in the current state but also in space and time. This study's insight will help increase the reliability of BGC models and predictions to society.

Acknowledgements

This study is supported by the Helmholtz Initiative and Networking Fund pilot project Uncertainty Quantification – From Data to Reliable Knowledge (Helmholtz-UQ). We acknowledge the high-performance computing resources of the North German Supercomputing Alliance (HLRN). We acknowledge the contribution of Pascal Richter and Marvin Thelen during the conceptualizing of the study. We thank Marvin Thelen for the initial code base for Monte Carlo sampling.

Supplementary Material

The Supplementary Material for this article can be found online at https://sesmo.org/article/view/18613/18119.

References

Albani, S., Mahowald, N. M., Perry, A. T., Scanza, R. A., Zender, C. S., Heavens, N. G., Maggi, V., Kok, J. F., & Otto-Bliesner, B. L. (2014). Improved dust representation in the Community Atmosphere Model. *Journal of Advances in Modeling Earth Systems*, 6(3):541–570.

Álvarez, E., Thoms, S., & Völker, C. (2018). Chlorophyll to Carbon Ratio Derived from a Global Ecosystem Model With Photodamage. *Global Biogeochemical Cycles*, 32(5):799–816.

Andersen, T. K., Bolding, K., Nielsen, A., Bruggeman, J., Jeppesen, E., & Trolle, D. (2021). How morphology shapes the parameter sensitivity of lake ecosystem models. *Environmental Modelling & Software*, 136:104945.

Anderson, T. R., Hessen, D. O., Mitra, A., Mayor, D. J., & Yool, A. (2013). Sensitivity of secondary production and export flux to choice of trophic transfer formulation in marine ecosystem models. *Journal of Marine Systems*, 125:41–53.

Baklouti, M., Faure, V., Pawlowski, L., & Sciandra, A. (2006). Investigation and sensitivity analysis of a mechanistic phytoplankton model implemented in a new modular numerical tool (Eco3M) dedicated to biogeochemical modelling. *Progress in Oceanography*, 71(1):34–58.

Baretta, J. W., Ebenhöh, W., & Ruardij, P. (1995). The European regional seas ecosystem model, a complex marine ecosystem model. *Netherlands Journal of Sea Research*, 33(3):233–246.

Behrenfeld, M. J. & Milligan, A. J. (2013). Photophysiological expressions of iron stress in phytoplankton. *Annual Review of Marine Science*, 5:217–46.

Boyle, E. A., Anderson, R. F., Cutter, G. A., Fine, R., Jenkins, W. J., & Saito, M. (2015). Introduction to the U.S. GEOTRACES North Atlantic Transect (GA-03): USGT10 and USGT11 cruises. *Deep Sea Research Part II: Topical Studies in Oceanography*, 116:1–5.

Bracis, C., Lehuta, S., Savina-Rolland, M., Travers-Trolet, M., & Girardin, R. (2020). Improving confidence in complex ecosystem models: The sensitivity analysis of an Atlantis ecosystem model. *Ecological Modelling*, 431:109133.

Broto, B., Bachoc, F., & Depecker, M. (2020). Variance reduction for estimation of Shapley Effects and adaptation to unknown input distribution. *SIAM/ASA Journal on Uncertainty Quantification*, 8(2):693–716.

Campbell, J. W. (1995). The lognormal distribution as a model for bio-optical variability in the sea. *Journal of Geophysical Research*, 100(C7):13237–13254.

Carroll, D., Menemenlis, D., Adkins, J. F., Bowman, K. W., Brix, H., Dutkiewicz, S., Fenty, I., Gierach, M. M., Hill, C., Jahn, O., Landschützer, P., Lauderdale, J. M., Liu, J., Manizza, M., Naviaux, J. D., Rödenbeck, C., Schimel, D. S., Van der Stocken, T., & Zhang, H. (2020). The ECCO-Darwin Data-Assimilative Global Ocean Biogeochemistry Model: Estimates of Seasonal to Multidecadal Surface Ocean pCO_2 and Air-Sea CO_2 Flux. *Journal of Advances in Modeling Earth Systems*, 12(10):e2019MS001888.

Chatterjee, S. (2020). A New Coefficient of Correlation. *Journal of the American Statistical Association*, 116(536):2009–2022.

Chenillat, F., Riviere, P., & Ohman, M. D. (2021). On the sensitivity of plankton ecosystem models to the formulation of zooplankton grazing. *PLoS One*, 16(5):e0252033.

Chien, C. T., Pahlow, M., Schartau, M., & Oschlies, A. (2020). Optimality-based non-Redfield plankton-ecosystem model (OPEM v1.1) in UVic-ESCM 2.9-Part 2: Sensitivity analysis and model calibration. *Geoscientific Model Development*, 13(10):4691–4712.

Coppola, L., Diamond, R. E., & Carval, T. (2021). Dyfamed observatory data. SEANOE.

Daines, S. J., Clark, J. R., & Lenton, T. M. (2014). Multiple environmental controls on phytoplankton growth strategies determine adaptive responses of the N : P ratio. *Ecology Letters*, 17(4):414–425.

Dowd, M., Jones, E., & Parslow, J. (2014). A statistical overview and perspectives on data assimilation for marine biogeochemical models. *Environmetrics*, 25(4):203–213.

Druon, J.-N. & Le Fèvre, J. (1999). Sensitivity of a pelagic ecosystem model to variations of process parameters within a realistic range. *Journal of Marine Systems*, 19(1):1–26.

Evelyn, J. L. & Michael, C. M. (1998). Microzooplankton herbivory and phytoplankton growth in the northwestern Sargasso Sea. *Aquatic Microbial Ecology*, 16(2):173–188.

Fennel, K. & Boss, E. (2003). Subsurface maxima of phytoplankton and chlorophyll: Steady-state solutions from a simple model. *Limnology and Oceanography*, 48(4):1521–1534.

Fennel, K., Gehlen, M., Brasseur, P., Brown, C. W., Ciavatta, S., Cossarini, G., Crise, A., Edwards, C. A., Ford, D., Friedrichs, M. A. M., Gregoire, M., Jones, E., Kim, H. C., Lamouroux, J., Murtugudde, R., Perruche, C., the GODAE OceanView Marine Ecosystem Analysis Prediction Task Team (2019). Advancing marine biogeochemical and ecosystem reanalyses and forecasts as tools for monitoring and managing ecosystem health. *Frontiers in Marine Science*, 6:89.

Fennel, K., Losch, M., Schroter, J., & Wenzel, M. (2001). Testing a marine ecosystem model: sensitivity analysis and parameter optimization. *Journal of Marine Systems*, 28(1-2):45–63.

Fennel, K., Mattern, J. P., Doney, S. C., Bopp, L., Moore, A. M., Wang, B., & Yu, L. (2022). Ocean biogeochemical modelling. *Nature Reviews Methods Primers*, 2(1):76.

Franks, P. J. S. (2002). NPZ models of plankton dynamics: Their construction, coupling to physics, and application. *Journal of Oceanography*, 58(2):379–387.

Gamboa, F., Gremaud, P., Klein, T., & Lagnoux, A. (2022). Global sensitivity analysis: A novel generation of mighty estimators based on rank statistics. *Bernoulli*, 28(4):2345–2374.

Geider, R. J. & La Roche, J. (1994). The role of iron in phytoplankton photosynthesis, and the potential for iron-limitation of primary productivity in the sea. *Photosynthesis Research*, 39(3):275–301.

Geider, R. J., MacIntyre, H. L., & Kana, T. M. (1997). Dynamic model of phytoplankton growth and acclimation: Responses of the balanced growth rate and the chlorophyll a:carbon ratio to light, nutrient-limitation and temperature. *Marine Ecology Progress Series*, 148(1-3):187–200.

Geider, R. J., MacIntyre, H. L., & Kana, T. M. (1998). A dynamic regulatory model of phytoplanktonic acclimation to light, nutrients, and temperature. *Limnology and Oceanography*, 43(4):679–694.

Glen, G. & Isaacs, K. (2012). Estimating Sobol sensitivity indices using correlations. *Environmental Modelling & Software*, 37:157–166.

Glover, D. M., Jenkins, W. J., & Doney, S. C. (2011). *Modeling Methods for Marine Science*. Cambridge University Press, Cambridge.

Guieu, C. & Blain, S. (2013). Concentrations of total dissolved iron measured on water bottle samples during THALASSA cruise PROSOPE.

Gupta, H. V. & Razavi, S. (2018). Revisiting the basis of sensitivity analysis for dynamical Earth System Models. *Water Resources Research*, 54(11):8692–8717.

Gutknecht, E., Reffray, G., Mignot, A., Dabrowski, T., & Sotillo, M. G. (2019). Modelling the marine ecosystem of Iberia–Biscay–Ireland (IBI) European waters for CMEMS operational applications. *Ocean Science*, 15(6):1489–1516.

Hauck, J., Volker, C., Wang, T., Hoppema, M., Losch, M., & Wolf-Gladrow, D. A. (2013). Seasonally different carbon flux changes in the Southern Ocean in response to the southern annular mode. *Global Biogeochem Cycles*, 27(4):1236–1245.

Hauck, J., Zeising, M., Le Quéré, C., Gruber, N., Bakker, D. C. E., Bopp, L., Chau, T. T. T., Gürses, O., Ilyina, T., Landschützer, P., Lenton, A., Resplandy, L., Rödenbeck, C., Schwinger, J., & Séférian, R. (2020). Consistency and challenges in the ocean carbon sink estimate for the global carbon budget. *Frontiers in Marine Science*, 7:571720.

Herman, J. & Usher, W. (2017). SALib: An open-source python library for sensitivity analysis. *The Journal of Open Source Software*, 2(9).

Hersbach, H., Bell, B., Berrisford, P., Hirahara, S., Horányi, A., Muñoz-Sabater, J., Nicolas, J., Peubey, C., Radu, R., Schepers, D., Simmons, A., Soci, C., Abdalla, S., Abellan, X., Balsamo, G., Bechtold, P., Biavati, G., Bidlot, J., Bonavita, M., De Chiara, G., Dahlgren, P., Dee, D., Diamantakis, M., Dragani, R., Flemming, J., Forbes, R., Fuentes, M., Geer, A., Haimberger, L., Healy, S., Hogan, R. J., Hólm, E., Janisková, M., Keeley, S., Laloyaux, P., Lopez, P., Lupu, C., Radnoti, G., de Rosnay, P., Rozum, I., Vamborg, F., Villaume, S., & Thépaut, J.-N. (2020). The ERA5 global reanalysis. *Quarterly Journal of the Royal Meteorological Society*, 146(730):1999–2049.

Hohn, S. (2009). *Coupling and decoupling of biogeochemical cycles in marine ecosystems*. Thesis, Fachbereich 2 Biologie.

Homma, T. & Saltelli, A. (1996). Importance measures in global sensitivity analysis of nonlinear models. *Reliability Engineering & System Safety*, 52(1):1–17.

Iooss, B., Da Veiga, S., Janon, A., & Pujol, G. (2022). sensitivity: Global Sensitivity Analysis of Model Outputs, R package version 1.27.1. Technical report, C-RAN.

Iooss, B. & Prieur, C. (2019). Shapley effects for sensitivity analysis with correlated inputs: Comparisons with Sobol' indices, numerical estimation and applications. *International Journal for Uncertainty Quantification*, 9(5):493–514.

Islam, A. & Karadogan, E. (2019). Sensitivity and uncertainty analysis of one-dimensional Tanaka and Liang-Rogers Shape Memory Alloy Constitutive Models. *Materials*, 12(10):1687.

Iwanaga, T., Usher, W., & Herman, J. (2022). Toward SALib 2.0: Advancing the accessibility and interpretability of global sensitivity analyses. *Socio-Environmental Systems Modelling*, 4:18155.

Ji, X. L., Liu, G. M., Gao, S., & Wang, H. (2015). Parameter sensitivity study of the biogeochemical model in the China coastal seas. *Acta Oceanologica Sinica*, 34(12):51–60.

Kalra, T. S., Aretxabaleta, A., Seshadri, P., Ganju, N. K., & Beudin, A. (2017). Sensitivity analysis of a coupled hydrodynamic-vegetation model using the effectively subsampled quadratures method (ESQM v5.2). *Geoscientific Model Development*, 10(12):4511–4523.

Karakuş, O., Völker, C., Iversen, M., Hagen, W., & Hauck, J. (2022). The role of zooplankton grazing and nutrient recycling for global ocean biogeochemistry and phytoplankton phenology. *Journal of Geophysical Research: Biogeosciences*, 127(10):e2022JG006798.

Kriest, I., Oschlies, A., & Khatiwala, S. (2012). Sensitivity analysis of simple global marine biogeochemical models. *Global Biogeochemical Cycles*, 26(2):GB2029.

Kucherenko, S., Feil, B., Shah, N., & Mauntz, W. (2011). The identification of model effective dimensions using global sensitivity analysis. *Reliability Engineering & System Safety*, 96(4):440-449.

Kucherenko, S. & Song, S. (2017). Different numerical estimators for main effect global sensitivity indices. *Reliability Engineering & System Safety*, 165:222–238.

Kucherenko, S., Tarantola, S., & Annoni, P. (2012). Estimation of global sensitivity indices for models with dependent variables. *Computer Physics Communications*, 183(4):937–946.

Kvale, K. F. & Meissner, K. J. (2017). Primary production sensitivity to phytoplankton light attenuation parameter increases with transient forcing. *Biogeosciences*, 14(20):4767–4780.

Large, W. G. & Yeager, S. G. (2008). The global climatology of an interannually varying air–sea flux data set. *Climate Dynamics*, 33(2-3):341–364.

Laufkötter, C., Vogt, M., Gruber, N., Aumont, O., Bopp, L., Doney, S. C., Dunne, J. P., Hauck, J., John, J. G., Lima, I. D., Seferian, R., & Völker, C. (2016). Projected decreases in future marine export production: the role of the carbon flux through the upper ocean ecosystem. *Biogeosciences*, 13(13):4023–4047.

Lauvset, S. K., Key, R. M., Olsen, A., van Heuven, S., Velo, A., Lin, X. H., Schirnick, C., Kozyr, A., Tanhua, T., Hoppema, M., Jutterstrom, S., Steinfeldt, R., Jeansson, E., Ishii, M., Perez, F. F., Suzuki, T., & Watelet, S. (2016). A new global interior ocean mapped climatology: the 1 degrees x 1 degrees GLODAP version 2. *Earth System Science Data*, 8(2):325–340.

Lavoie, D., Lambert, N., Starr, M., Chassé, J., Riche, O., Le Clainche, Y., Azetsu-Scott, K., Béjaoui, B., Christian, J. R., & Gilbert, D. (2021). The gulf of St. Lawrence biogeochemical model: A modelling tool for fisheries and ocean management. *Frontiers in Marine Science*, 8:732269.

Le Quéré, C., Buitenhuis, E. T., Moriarty, R., Alvain, S., Aumont, O., Bopp, L., Chollet, S., Enright, C., Franklin, D. J., Geider, R. J., Harrison, S. P., Hirst, A. G., Larsen, S., Legendre, L., Platt, T., Prentice, I. C., Rivkin, R. B., Sailley, S., Sathyendranath, S., Stephens, N., Vogt, M., & Vallina, S. M. (2016). Role of zooplankton dynamics for Southern Ocean phytoplankton biomass and global biogeochemical cycles. *Biogeosciences*, 13(14):4111–4133.

Leles, S. G., Polimene, L., Bruggeman, J., Blackford, J., Ciavatta, S., Mitra, A., & Flynn, K. J. (2018). Modelling mixotrophic functional diversity and implications for ecosystem function. *Journal of Plankton Research*, 40(6):627–642.

Makler-Pick, V., Gal, G., Gorfine, M., Hipsey, M. R., & Carmel, Y. (2011). Sensitivity analysis for complex ecological models - A new approach. *Environmental Modelling & Software*, 26(2):124–134.

Mamnun, N., Völker, C., Vrekoussis, M., & Nerger, L. (2022). Uncertainties in ocean biogeochemical simulations: Application of ensemble data assimilation to a one-dimensional model. *Frontiers in Marine Science*, 9:980388.

Marshall, J., Adcroft, A., Hill, C., Perelman, L., & Heisey, C. (1997). A finite-volume, incompressible Navier Stokes model for studies of the ocean on parallel computers. *Journal of Geophysical Research-Oceans*, 102(C3):5753–5766.

Martiny, A. C., Vrugt, J. A., Primeau, F. W., & Lomas, M. W. (2013). Regional variation in the particulate organic carbon to nitrogen ratio in the surface ocean. *Global Biogeochemical Cycles*, 27(3):723–731.

Marty, J. C. (2002). The DYFAMED time-series program (French-JGOFS). *Deep-Sea Research Part II -Topical Studies in Oceanography*, 49(11):1963–1964.

Marty, J.-C., Garcia, N., & Raimbault, P. (2008). Phytoplankton dynamics and primary production under late summer conditions in the NW Mediterranean Sea. *Deep Sea Research Part I: Oceanographic Research Papers*, 55(9):1131–1149.

Mayot, N., Nival, P., & Levy, M. (2020). Primary production in the ligurian sea. In Migon, C., Nival, P., & Sciandra, A., editors, *The Mediterranean Sea in the Era of Global Change 1: 30 Years of Multidisciplinary Study of the Ligurian Sea*, Wiley Online Books, pages 139–164. Wiley-VCH GmbH, Weinheim, Germany.

Morris, M. D. (1991). Factorial sampling plans for preliminary computational experiments. *Technometrics*, 33(2):161–174.

Nelson, D. M. & Brzezinski, M. A. (1997). Diatom growth and productivity in an oligo-trophic midocean gyre: A 3-yr record from the Sargasso Sea near Bermuda. *Limnology and Oceanography*, 42(3):473–486.

Ökten, G. & Liu, Y. (2021). Randomized quasi-Monte Carlo methods in global sensitivity analysis. *Reliability Engineering & System Safety*, 210:107520.

Olsen, A., Brown, K. R., Chierici, M., Johannessen, T., & Neill, C. (2008). Sea-surface CO_2 fugacity in the subpolar North Atlantic. *Biogeosciences*, 5(2):535–547.

Orr, J. C., Najjar, R. G., Aumont, O., Bopp, L., Bullister, J. L., Danabasoglu, G., Doney, S. C., Dunne, J. P., Dutay, J. C., Graven, H., Griffies, S. M., John, J. G., Joos, F., Levin, I., Lindsay, K., Matear, R. J., McKinley, G. A., Mouchet, A., Oschlies, A., Romanou, A., Schlitzer, R., Tagliabue, A., Tanhua, T., & Yool, A. (2017). Biogeochemical protocols and diagnostics for the CMIP6 Ocean Model Intercomparison Project (OMIP). *Geoscientific Model Development*, 10(6):2169–2199.

Owen, A. B., Dick, J., & Chen, S. (2014). Higher order Sobol' indices. *Information and Inference: A Journal of the IMA*, 3(1):59–81.

Owen, A. B. & Prieur, C. (2017). On Shapley value for measuring importance of dependent inputs. *SIAM/ASA Journal on Uncertainty Quantification*, 5(1):986–1002.

Plischke, E., Borgonovo, E., & Smith, C. L. (2013). Global sensitivity measures from given data. *European Journal of Operational Research*, 226(3):536–550.

Popova, E. E., Coward, A. C., Nurser, G. A., de Cuevas, B., Fasham, M. J. R., & Anderson, T. R. (2006). Mechanisms controlling primary and new production in a global ecosystem model – part I: Validation of the biological simulation. *Ocean Science*, 2(2):249–266.

Prieur, C., Viry, L., Blayo, E., & Brankart, J. M. (2019). A global sensitivity analysis approach for marine biogeochemical modeling. *Ocean Modelling*, 139:101402.

Razavi, S. & Gupta, H. V. (2015). What do we mean by sensitivity analysis? The need for comprehensive characterization of "global" sensitivity in Earth and environmental systems models. *Water Resources Research*, 51(5):3070–3092.

Razavi, S., Jakeman, A., Saltelli, A., Prieur, C., Iooss, B., Borgonovo, E., Plischke, E., Lo Piano, S., Iwanaga, T., Becker, W., Tarantola, S., Guillaume, J. H. A., Jakeman, J., Gupta, H., Melillo, N., Rabitti, G., Chabridon, V., Duan, Q. Y., Sun, X. F., Smith, S., Sheikholeslami, R., Hosseini, N., Asadzadeh, M., Puy, A., Kucherenko, S., & Maier, H. R. (2021). The future of sensitivity analysis: An essential discipline for systems modeling and policy support. *Environmental Modelling & Software*, 137:104954.

Redfield, A. C. (1934). On the proportions of organic derivations in sea water and their relation to the composition of plankton. In Daniel, R., editor, *James Johnstone Memorial Volume*, pages 176–192. University Press of Liverpool, Liverpool, UK.

Saltelli, A. & Funtowicz, S. (2014). When all models are wrong. *Issues in Science and Technology*, 30(02).

Saltelli, A., Ratto, M., Andres, T., Campolongo, F., Cariboni, J., Gatelli, D., Saisana, M., & Tarantola, S. (2008). *Global sensitivity analysis: the primer*. John Wiley & Sons.

Saltelli, A., Tarantola, S., Campolongo, F., & Ratto, M. (2004). *Sensitivity Analysis in Practice: A Guide to Assessing Scientific Models*. John Wiley & Sons Ltd, West Sussex.

Sankar, S., Polimene, L., Marin, L., Menon, N. N., Samuelsen, A., Pastres, R., & Ciavatta, S. (2018). Sensitivity of the simulated oxygen minimum zone to biogeochemical processes at an oligotrophic site in the arabian sea. *Ecological Modelling*, 372:12–23.

Schartau, M., Wallhead, P., Hemmings, J., Loptien, U., Kriest, I., Krishna, S., Ward, B. A., Slawig, T., & Oschlies, A. (2017). Reviews and syntheses: parameter identification in marine planktonic ecosystem modelling. *Biogeosciences*, 14(6):1647–1701.

Scott, V., Kettle, H., & Merchant, C. J. (2011). Sensitivity analysis of an ocean carbon cycle model in the North Atlantic: an investigation of parameters affecting the air-sea CO_2 flux, primary production and export of detritus. *Ocean Science*, 7(3):405–419.

Sheikholeslami, R., Gharari, S., Papalexiou, S. M., & Clark, M. P. (2021). VISCOUS: A variance-based sensitivity analysis using copulas for efficient identification of dominant hydrological processes. *Water Resources Research*, 57(7):e2020WR028435.

Sobol, I. M. (1993). Sensitivity estimates for nonlinear mathematical model. *Mathematical Modeling and Computational Experiment*, 1(4):8.

Sobol', I. M. (2001). Global sensitivity indices for nonlinear mathematical models and their Monte Carlo estimates. *Mathematics and Computers in Simulation*, 55(1-3):271–280.

Sobol', I. M. & Kucherenko, S. (2009). Derivative based global sensitivity measures and their link with global sensitivity indices. *Mathematics and Computers in Simulation*, 79(10):3009–3017.

Sobol', I. M., Tarantola, S., Gatelli, D., Kucherenko, S. S., & Mauntz, W. (2007). Estimating the approximation error when fixing unessential factors in global sensitivity analysis. *Reliability Engineering & System Safety*, 92(7):957–960.

Sobol', I. M. & Kucherenko, S. (2010). Derivative based global sensitivity measures. *Procedia - Social and Behavioral Sciences*, 2(6):7745–7746.

Steinberg, D. K., Carlson, C. A., Bates, N. R., Johnson, R. J., Michaels, A. F., & Knap, A. H. (2001). Overview of the US JGOFS Bermuda Atlantic Time-series Study (BATS): a decade-scale look at ocean biology and biogeochemistry. *Deep Sea Research Part II: Topical Studies in Oceanography*, 48(8-9):1405–1447.

Steinberg, D. K. & Landry, M. R. (2017). Zooplankton and the ocean carbon cycle. *Annual Review of Marine Science*, 9:413–444.

Sweeney, E. N., McGillicuddy, D. J., & Buesseler, K. O. (2003). Biogeochemical impacts due to mesoscale eddy activity in the Sargasso Sea as measured at the Bermuda Atlantic Time-series Study (BATS). *Deep Sea Research Part II: Topical Studies in Oceanography*, 50(22):3017–3039.

Tarantola, S., Gatelli, D., & Mara, T. A. (2006). Random balance designs for the estimation of first order global sensitivity indices. *Reliability Engineering & System Safety*, 91(6):717–727.

Thelen, M. C. B. (2021). Quantication of uncertainties and determination of sensitivities for biogeochemical ocean simulation. Master's thesis, RWTH Aachen University, Aachen, Germany.

Tjiputra, J. F., Polzin, D., & Winguth, A. M. E. (2007). Assimilation of seasonal chlorophyll and nutrient data into an adjoint three-dimensional ocean carbon cycle model: Sensitivity analysis and ecosystem parameter optimization. *Global Biogeochemical Cycles*, 21(1).

Tjiputra, J. F. & Winguth, A. M. E. (2008). Sensitivity of sea-to-air co_2 flux to ecosystem parameters from an adjoint model. *Biogeosciences*, 5(2):615–630.

Tommasi, D., Stock, C. A., Hobday, A. J., Methot, R., Kaplan, I. C., Eveson, J. P., Holsman, K., Miller, T. J., Gaichas, S., Gehlen, M., Pershing, A., Vecchi, G. A., Msadek, R., Delworth, T., Eakin, C. M., Haltuch, M. A., Seferian, R., Spillman, C. M., Hartog, J. R., Siedlecki, S., Samhouri, J. F., Muhling, B., Asch, R. G., Pinsky, M. L., Saba, V. S., Kapnick, S. B., Gaitan, C. F., Rykaczewski, R. R., Alexander, M. A., Xue, Y., Pegion, K. V., Lynch, P., Payne, M. R., Kristiansen, T., Lehodey, P., & Werner, F. E. (2017). Managing living marine resources in a dynamic environment: The role of seasonal to decadal climate forecasts. *Progress in Oceanography*, 152:15–49.

van Rossum, G. & the Python development team (2022). The Python Language Reference; Release 3.9.16.

Wagener, T. & Pianosi, F. (2019). What has global sensitivity analysis ever done for us? A systematic review to support scientific advancement and to inform policy-making in earth system modelling. *Earth-Science Reviews*, 194:1–18.

Wang, S., Flipo, N., & Romary, T. (2018). Time-dependent global sensitivity analysis of the C-RIVE biogeochemical model in contrasted hydrological and trophic contexts. *Water Research*, 144:341–355.

Ward, B. A., Dutkiewicz, S., Jahn, O., & Follows, M. J. (2012). A size-structured food-web model for the global ocean. *Limnology and Oceanography*, 57(6):1877–1891.